Inorganic Chemistry

pubs.acs.org/IC

Article

On the Prediction of Spectroscopic Fingerprints of Co^{2+} Complexes Relevant for the ZIF Nucleation Process

Liesbeth De Bruecker, Matthias Filez, and Veronique Van Speybroeck*

Cite This: https://doi.org/10.1021/acs.inorgchem.3c01355

Read Online

ACCESS | Metrics & More | Article Recommendations | Supporting Information

ABSTRACT: The nucleation process of zeolitic imidazolate frameworks (ZIFs) is to date not completely understood. Recently, it has been found that, during the formation of Co-ZIF-67, after mixing imidazole-type ligands with octahedral precursors containing oxygen-coordinated ligands, a metal−organic pool with a diversity of transition metal complexes (TMCs) is formed showing fingerprints of octahedral and tetrahedral Co^{2+} complexes with both types of ligands [Filez, M. et al. *Cell Rep. Phys. Sci.* **2021**, *2*, 100680]. In order to further unravel this process, we aim to characterize the d−d transitions of the TMCs and focus on their number, intensity, and position, which change during the process and can thus serve as a fingerprint for the formed species. It was previously shown that the number of ligands and symmetry has a detrimental influence on the ground state properties of Co^{2+} TMCs. Herein, we investigate how far excited state properties of TMCs relevant during nanoporous formation processes can be predicted by time-dependent density functional theory (TDDFT) and ligand field density functional theory (LFDFT). As TMCs are known to be challenging systems with possibly degenerate ground states and double excitations, we first investigate the performance of both techniques on first-row octahedral aqua-complexes. With this knowledge, we then focus on tetrahedral Co^{2+} complexes with aqua and imidazole-type ligands in order to investigate in how far we can propose a spectroscopic fingerprint that allows us to follow the Co^{2+} complexes during the formation of Co-ZIF-67. The results of TDDFT and LFDFT are qualitatively in agreement and provide complementary information. We found that various features can be used to distinguish between the species. However, as LFDFT is not suited for TMCs possessing the extended imidazole-type ligands and double and spin-flip states are not included in TDDFT, both techniques need to be complemented with more advanced methods to obtain complete insight into the d−d excitations of TMCs with imidazole ligands. Therefore, we particularly explored ab initio ligand field theory, which is capable of describing double excitations and is, in contrast to LFDFT, suitable for TMCs with extended ligands.

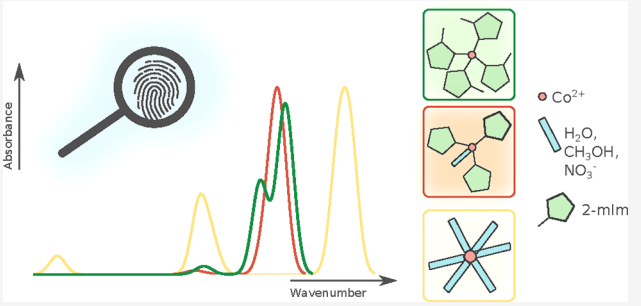

1. INTRODUCTION

The nucleation process of zeolitic imidazolate frameworks (ZIFs) has, until now, not yet completely understood. This makes the exploration for materials tailored for specific applications in various domains very burdensome.[1−3] Recently, a combined experimental-computational study[4] investigated the nucleation of Co-ZIF-67, formed by mixing $Co(NO_3)_2 \cdot 6H_2O$ and 2-methylimidazole (2-mIm). The former contains predominantly octahedral transition metal complexes (TMCs) with aqua ligands. It has been revealed that after mixing a pool with a variety of TMCs is formed because of ligand elimination and substitution reactions, as shown in Figure 1. The transformation of octahedral precursors to five- and finally four-coordinated complexes is accompanied by an exchange and elimination of aqua ligands with 2-mIm ligands. For the sake of fully understanding this intricate process, we would like to study the changes in the UV−vis spectrum as this was also experimentally measured in the paper of Filez et al. to identify the various species in the nucleation process.[4] More specifically, we will concentrate on the number, intensity, and position of the d−d transitions, as they alter during the nucleation and can therefore act as a fingerprint. Previously, we studied the ground state (GS) properties of six-, five-, and four-coordinated Co^{2+} aqua-complexes[5] and concluded that the d-orbital splitting is characteristic for the number of ligands coordinated to the transition metal (TM) and for the symmetry of the complex. We also investigated the performance of different techniques based on density functional theory (DFT) to calculate the d-orbital splitting quantitatively. In this work, we complement our investigation toward the d−d excitations of six- and four-coordinated Co^{2+} complexes as Filez et al. found that after mixing $Co(NO_3)_2 \cdot 6H_2O$ and 2-

Received: April 26, 2023

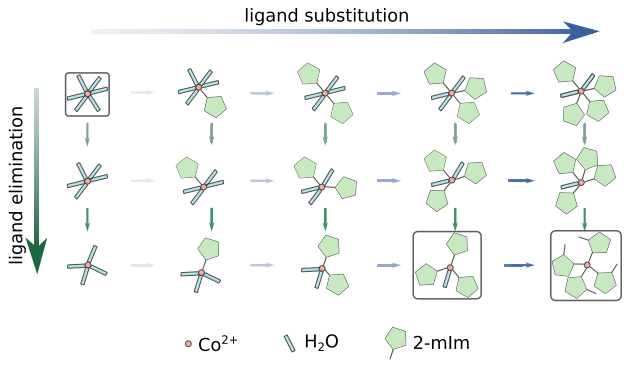

Figure 1. Reaction network of ligand elimination and substitution reactions leading to fast pre-equilibrium formation toward a metal–organic pool. The complexes which are mainly present after mixing according to ref 4 are indicated in gray. These include octahedral Co^{2+} complexes with six aqua ligands and two types of tetrahedral structures, one with three 2-mIm ligands and one aqua ligand and the other with four 2-mIm ligands. Note that in practice methanol and to a lesser extent NO_3^- can also act as ligands. Figure adapted from ref 4 with permission of Elsevier, Copyright 2021.

mIm, the system mainly consists of $[Co(OR)_6]^{2+}$, $[Co(2\text{-}mIm)_3(OR)]^{2+}$, and $[Co(2\text{-}mIm)_4]^{2+}$ complexes.[4] Remark that here not only aqua ligands but also other ligands coordinating with oxygen to the TM, like methanol or NO_3^-. Note that it is less probable for the latter to directly coordinate to the TM as it will likely be replaced by the stronger aqua ligand. However, NO_3^- can appear in the second solvation shell and as such counterbalances the positive charge of the complex. In this work, we only consider aqua ligands in order to minimize the complexity of the system and to be able to compare the results to literature data.[6−9] Nevertheless, we thereby neglect the possible symmetry breaking caused by, for example, methanol compared to water. The studied complexes are indicated with gray in Figure 1. The excited states (ESs) are calculated via time-dependent DFT (TDDFT) and the ligand field (LFDFT). The computational spectra can then be compared to experimental data in order to put forward a fingerprint for the nucleation process of ZIFs.

It is generally known that the calculation of ESs in TMCs is not a trivial task and poses various challenges for current computational techniques.[10−13] Indeed, there might be numerous ESs lying closely together, some of which are double excitations. Furthermore, degeneracies in the ground or excited states may occur. A large body of literature is available on the usage of various electronic structure methods, including computationally very expensive techniques, for the calculations of ESs in small octahedral complexes.[6−8,14] As within this work, we are interested not only in aqua-complexes but also in more complex ligands relevant for the nucleation process; not all techniques proposed thus far are computationally feasible. Therefore, within the first part of this paper, we give more fundamental insights by unraveling the difficulties for the calculation of ESs in octahedral TMCs with aqua ligands and first-row divalent TMs in a methanol environment. Furthermore, the advantages and disadvantages of two computational techniques based on DFT, i.e., time-dependent DFT (TDDFT) and ligand field DFT (LFDFT), are discussed. In the second part, we return our focus to the nucleation process of Co-ZIF-67 and compare our computational results for octahedral Co^{2+} aqua-complexes and tetrahedral Co^{2+} complexes containing 2-mIm and aqua ligands with the experimental work of Filez et al.[4] in order to come up with a spectroscopic fingerprint. In addition, as will become clear in section 3, the LFDFT results are difficult to interpret for complexes with extended imidazole-type ligands. Therefore, some ab initio LFT (AILFT) calculations have been performed too.

2. CHALLENGES OF d–d EXCITATIONS IN AQUA-COMPLEXES FOR TDDFT AND LFDFT

2.1. Using Tanabe–Sugano Diagrams for the Description of d–d Excitations in TMCs. As octahedral and tetrahedral systems will play a major role in this work, the d-orbital splitting as predicted by crystal field theory (CFT) is shown in Figure 2, in which we also introduced the labeling of

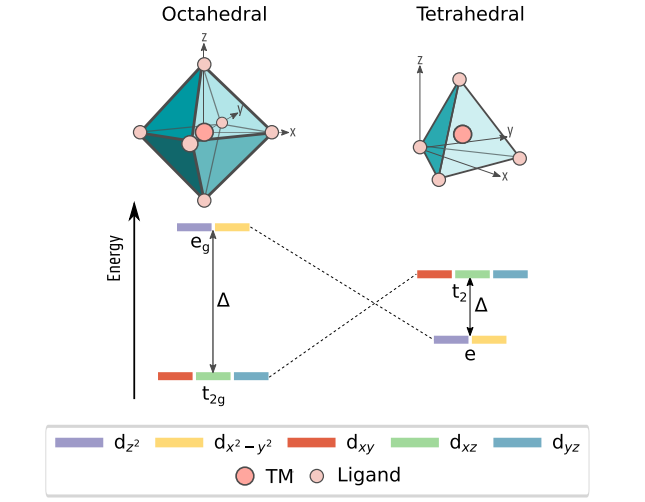

Figure 2. d-Orbital splitting in complexes with octahedral and tetrahedral symmetry. The splitting between the two orbital sets is denoted by Δ. The labeling of the d-orbitals is also indicated.

the orbital sets. In an octahedral ligand field, the d-orbitals of a TM split into t_{2g} and e_g set. Tetrahedral complexes bear a lot of similarities with octahedral complexes since both point groups are cubic. However, as the ligands are now situated in between the coordinate axes compared to at the coordinate axes as in octahedral complexes, the d-orbital splitting pattern is reversed.

Tanabe–Sugano (TS) diagrams are very helpful to predict and label the transitions between the d-orbitals in octahedral and tetrahedral TMCs.[15,16] They show the excitation energy E as a function of ligand field splitting Δ, where both are scaled by the Racah parameter B. The TS diagram for octahedral Co^{2+} complexes with d^7 electron configuration is shown in the left side of Figure 3, where only the lowest energy states are included, which are relevant in the remainder of this work. In the weak field limit situated at the left of the diagram, the lowest energy terms ^4F, ^4P, and ^2G are indicated in light purple, dark purple, and green, respectively. Under the influence of an increasing ligand field, these terms split in several states. The GS for $[Co(H_2O)_6]^{2+}$ is the high spin (HS) $^4T_{1g}(F)$ state corresponding to the $t_{2g}^5e_g^2$ electron configuration. The three microstates with maximal spin projection associated with this configuration are shown in the bottom row on the right and are labeled a–c. The meaning of the line style of the boxes will be explained later. From this GS, there are three spin-allowed and one spin-forbidden transitions in the low-energy range. First of all, one t_{2g}-electron can excite to an e_g-orbital, resulting

https://doi.org/10.1021/acs.inorgchem.3c01355
Inorg. Chem. XXXX, XXX, XXX−XXX

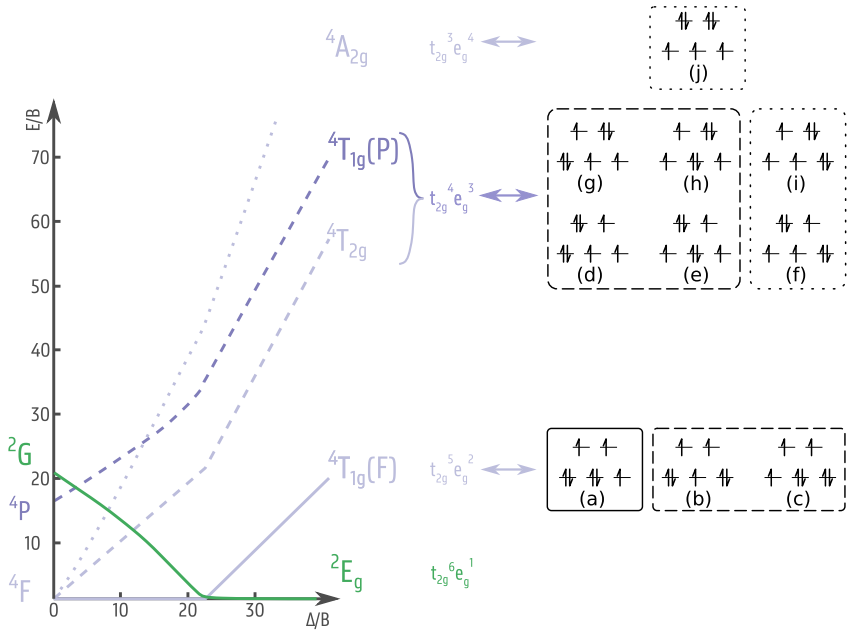

Figure 3. TS diagram for octahedral d^7 complexes in which the energy E is plotted as a function of the ligand field splitting Δ, both scaled by the Racah parameter B. Quartet and doublet states are indicated with purple and green lines, respectively. Dashed and dotted lines represent single and double excitations. On the right, the corresponding microstates with maximal spin projection are indicated for the quartet states and are labeled a−j. In DFT, one microstate is chosen as the GS reference, of which the box is denoted with a solid line. Single excitations from this GS reference are characterized with dashed lines and double ESs with dotted lines.

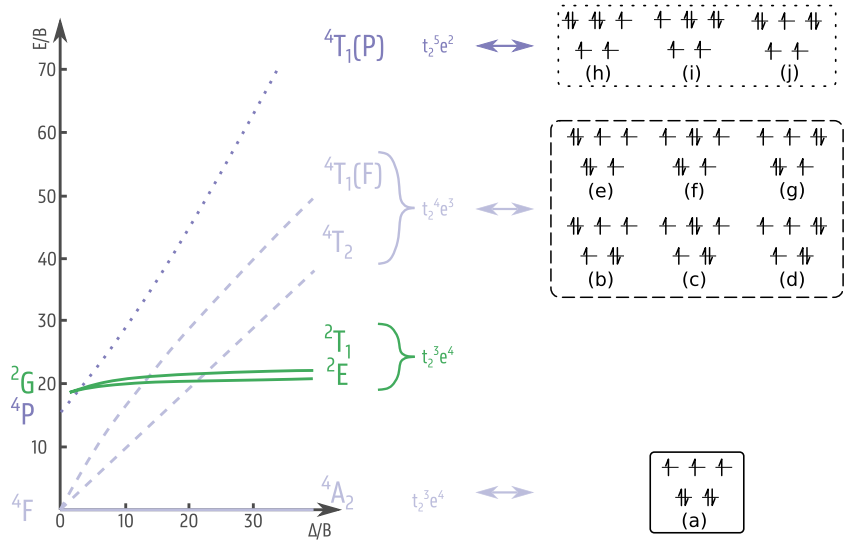

Figure 4. TS diagram for octahedral d^3 and tetrahedral d^7 complexes in which the energy E is plotted as a function of the ligand field splitting Δ, both scaled by the Racah parameter B. Quartet and doublet states are indicated with purple and green lines, respectively. Dashed and dotted lines represent single and double excitations. On the right, the corresponding microstates with maximal spin projection are indicated for the quartet states and are labeled a−j. In DFT, one microstate is chosen as the GS reference, of which the box is denoted with a solid line. Single excitations from this GS reference are characterized with dashed lines and double ESs with dotted lines.

in the $t_{2g}^4e_g^3$ electron configuration, indicated by the $^4T_{2g}$ and $^4T_{1g}(P)$ states being light and dark purple, respectively. These states are reached via a single excitation and are therefore indicated with a dashed line. Six possible microstates with maximal spin projection can be drawn, d−i. When another t_{2g}-electron is transferred to an e_g-orbital, $t_{2g}^3e_g^4$ is obtained, corresponding to the $^4A_{2g}$ term. This is a double excitation, as now two electrons are excited, which is indicated in the TS diagram with a dotted line. There is only one microstate with maximal spin projection, namely j. The lowest spin-forbidden excitation is obtained when an e_g-electron is transferred toward a t_{2g}-orbital followed by a spin flip, resulting in the ^2E_g state with $t_{2g}^6e_g^1$ configuration as presented in green.

It is important to note that all of these transitions are Laporte forbidden since they conserve the parity in a complex with a center of symmetry.[17] Therefore, the d−d absorption bands are expected to be weak for octahedral complexes. As spin-forbidden transitions are presumed to be even less intense, we will focus on only spin-allowed excitations. Furthermore, one must keep in mind that this description

https://doi.org/10.1021/acs.inorgchem.3c01355
Inorg. Chem. XXXX, XXX, XXX−XXX

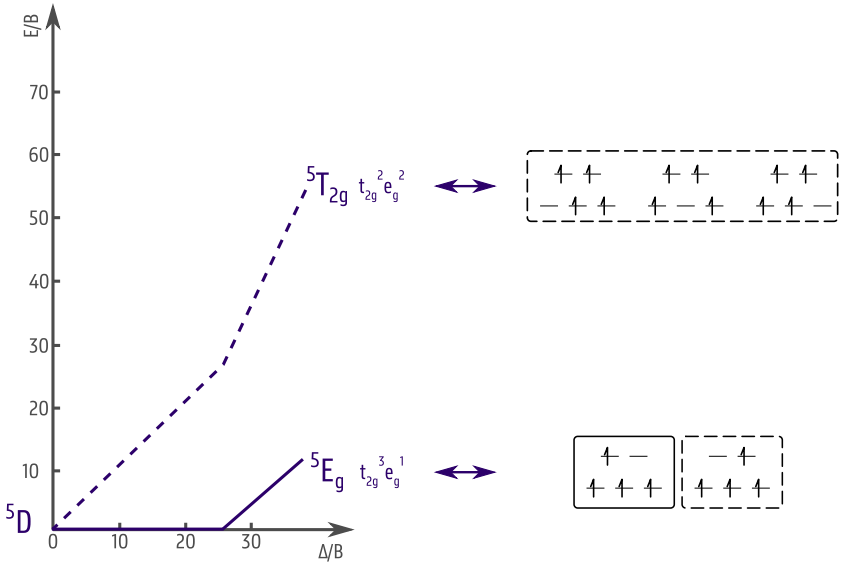

Figure 5. TS diagram for octahedral d^4 complexes in which energy E is plotted as a function of ligand field splitting Δ, both scaled by the Racah parameter B. Quintet states are indicated with purple lines. The dashed line represents a single excitation. On the right, the corresponding microstates with maximal spin projection are indicated. In DFT, one microstate is chosen as the GS reference, of which the box is denoted with a solid line. Single excitations from this GS reference are characterized with dashed lines.

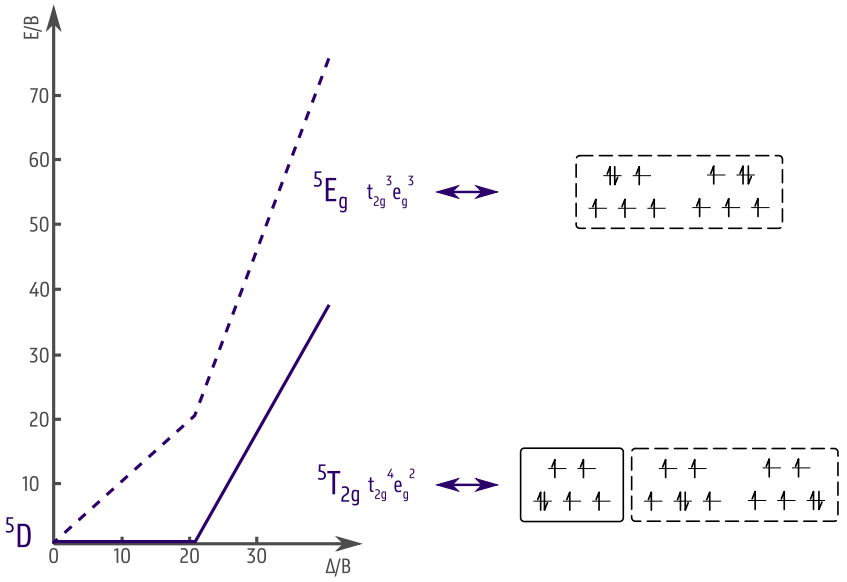

Figure 6. TS diagram for octahedral d^6 complexes in which the energy E is plotted as a function of the ligand field splitting Δ, both scaled by the Racah parameter B. Quintet states are indicated with purple lines. The dashed line represents a single excitation. On the right, the corresponding microstates with maximal spin projection are indicated. In DFT, one microstate is chosen as the GS reference, of which the box is denoted with a solid line. Single excitations from this GS reference are characterized with dashed lines.

applies to TMCs with perfect octahedral symmetry. When geometrical distortions occur in the complex, some of the states split into substates, leading to more peaks in the spectra, as will be observed in the remainder of the manuscript.

The diagrams for d^2, d^3, d^4, d^6, and d^8 complexes are presented in Figures S1, 4, 5, 6, and S2, respectively. Note that the TS diagrams for octahedral d^n complexes are identical with those of tetrahedral d^{10-n} systems. Indeed, as stated before, the splitting pattern for the d-orbitals in a tetrahedral field is the inverse of that in an octahedral field. As such, the occupation of the t_2 and e orbital sets are similar for octahedral d^n and tetrahedral d^{10-n} complexes, resulting in analogous TS diagrams. The only difference is in the labeling of the states. As octahedral complexes have a center of symmetry, the subscript g or u, indicating the symmetry with respect to an inversion, is included, whereas this is not the case for tetrahedral systems.

As mentioned above, tetrahedral d^7 complexes will play a major role in this work. Hence, we also discuss its TS diagram presented in Figure 4. The GS is now $^4A_2$, corresponding to the $t_2^3e^4$ electron configuration. Again three spin-allowed transitions with low energy occur. When an e-electron gets excited toward a t_2-orbital, the $^4T_2$ and $^4T_1(F)$ terms are obtained, indicated in light purple with dashed lines. When another e-electron is transferred to a t_2-orbital, we arrive at the $t_2^5e^2$ configuration, labeled with $^4T_1(P)$. This double excitation

https://doi.org/10.1021/acs.inorgchem.3c01355
Inorg. Chem. XXXX, XXX, XXX−XXX

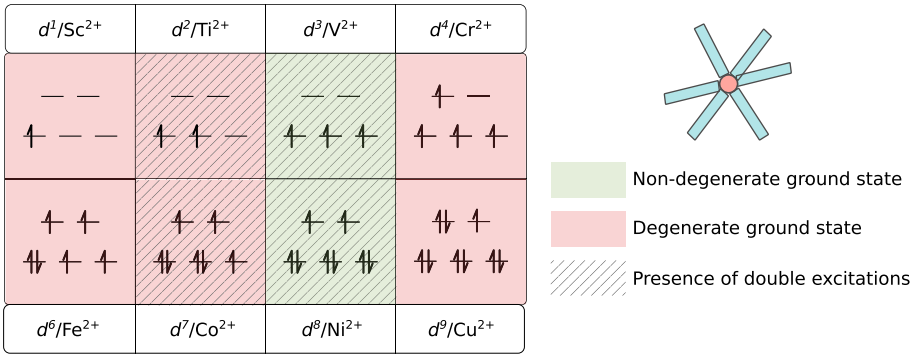

Figure 7. Overview of the challenges encountered for the calculation of ESs in octahedral first-row TMCs. The electron configuration of the high-spin GS is shown. Green/red indicates that the GS is nondegenerate/degenerate and diagonal stripes denote the presence of double excitations.

is again indicated with a dotted line. The microstates with maximal spin projection are also drawn for each electron configuration. In contrast to the octahedral complexes, tetrahedral systems lack a center of symmetry; therefore, they have much more intense absorption bands.

These TS diagrams are helpful for the study of d−d excitations in TMCs as they show for each electron configuration the number of ESs and provide a way to label them. Furthermore, the link with the corresponding electron configurations will also be of use to interpret the results obtained from TDDFT and to understand its deficiencies.

2.2. TDDFT versus LFDFT. An extensive body of literature on octahedral aqua-complexes with first-row TMs is already available.[6−8,14] Therefore, it is important to give some positioning of this work with respect to the literature. Neese et al. tested complete active space self-consistent field (CASSCF) and spectroscopy oriented configuration interaction (SORCI) on these challenging systems and concluded that the SORCI method on top of state-averaged CASSCF calculations yields good results.[6] Multireference ab initio techniques such as CASSCF, complete active space second-order perturbation theory (CASPT2), and multireference configuration interaction (MRCI) have been employed by Yang et al.[7] This study was followed by the work of Vlahovic et al., who compared TDDFT and LFDFT results.[8] They reported LFDFT to be the preferred method, as TDDFT only yields acceptable results for d^2 and d^4 TMCs. The rather poor performance of TDDFT was linked to the fact that double excitations are not covered and that orbital relaxation, which plays an important role when the ES only depends on the ligand field splitting, is neglected. Finally, Radoń et al. performed high-level multireference CASPT2 and second order n-electron valence state perturbation theory (NEVPT2).[14] They retrieved excellent results by explicitly including the second solvation shell and by adequately choosing the active space and extrapolating the energetics to the complete basis set limit. In the previous works, the computational techniques were quantitatively tested against experimental results and high-level ab initio calculations.[9,18−20]

With this work, we make a contribution to the previous studies by performing a comparison between results obtained from TDDFT and LFDFT calculations. Another DFT-based technique, which is, in contrast to TDDFT, capable to describe double excitations is constricted *n*th order variational DFT (CV(*n*)-DFT).[21−24] Nevertheless, to the best of our knowledge, its current implementation does not support unrestricted calculations and can, therefore, only be used for closed shell systems. Hereby, we want to emphasize that our goal is to find trends that can be helpful to unravel the nucleation process of ZIFs. Hence, we will also calculate spectra of Co^{2+} complexes with more complex ligands than water. In this sense, it is not possible to perform some of the very expensive levels of theory used in previous studies. First, we will critically evaluate how far computationally cheaper methods are able to give a qualitative correct picture for the series of first-row octahedral aqua-complexes. At second instance, we will use this knowledge to acquire some insights into the UV−vis spectra of Co^{2+} complexes observed during the nucleation process. Theretofore, we applied techniques based on DFT to calculate the ESs of octahedral and tetrahedral Co^{2+} complexes. These methods give a good balance between accuracy and computational cost, at least for typical, simple systems.[25] However, care must be taken when considering more challenging systems like TMCs. In addition, we will also briefly investigate the performance of AILFT for these TMCs.[26,27]

The GS reference, from which ESs are determined, can be obtained from average of configuration (AOC) or unrestricted DFT (UDFT) calculations as studied in our previous work.[5] In the former, the d-electrons are distributed evenly among the five molecular orbitals dominated by d-orbitals, resulting in a spin-restricted self-consistent field DFT calculation with fractional occupation numbers. In the latter, a spin-unrestricted calculation is performed with integer occupation numbers. In the following, we discuss how ESs can be determined via both techniques.

When starting from an AOC reference, multiplet energies can be obtained by calculating the energies of suitable determinants.[28] Although this method has been extended by Daul,[29] it remains limited as mixing between states is not included. Therefore, we will examine LFDFT, which has been introduced by Atanasov et al.[30−33] Indeed, the Kohn−Sham (KS)-orbitals obtained from an AOC calculation are ideally suited for techniques in which electron−electron repulsion is treated within full spherical symmetry, like for example in CFT. In LFDFT, the LF parameters are not determined by making use of experimental input, as is usually done in CFT, but they are obtained solely based on DFT calculations. In this way, the multiplet energy levels of a given electron configuration can be determined. The key feature of this technique is that both dynamical correlation, via the DFT exchange-correlation potential, and nondynamical correlation, via configuration interaction within the active space of KS orbitals with dominant d-character, are taken into account. LFDFT can calculate oscillator strengths only between states

https://doi.org/10.1021/acs.inorgchem.3c01355
Inorg. Chem. XXXX, XXX, XXX−XXX

coming from different electron configurations. The d−d transitions studied in this work come from the same electron configuration and are hence assumed to be Laporte forbidden. Nevertheless, we will show by using TDDFT that the oscillator strengths for the d−d transitions in TMCs that are not perfectly octahedral are different from zero as they are not completely Laporte forbidden.

When the GS reference is obtained from UDFT, the most popular technique to determine ESs is TDDFT[34] within the linear-response approach as developed by Casida.[35] Usually, the adiabatic approximation is applied in which the time-dependent exchange correlation potential is approximated by a GS one.[36,37] This black box technique has already been widely used for a broad area of systems, ranging from organic[38,39] and inorganic[40−44] molecules[36,45−48] to the very challenging TMCs.[48−50] However, we have to pay attention to analyzing the results for TMCs. Sometimes, the fact that the GS is not described correctly in DFT can be reflected in the wrong characterization of the ESs. For example, Deeth et al. found that in tetrahedral Pd complexes, the d-orbital splitting is predicted incorrectly by DFT, which is reflected in the ESs.[51] In our previous paper, we found that for the six-coordinated complexes the order of d-orbitals within the t_{2g} or e_g set is sometimes interchanged in the AOC and UDFT calculations due to the different electron occupations, resulting in different interelectron repulsions. However, no mixing between the two orbital sets occurs. Furthermore, we observed that the gap between the occupied and unoccupied orbitals is overestimated by UDFT. We will study in this work in how far these discrepancies are reflected in the ESs.

To set the scene, Figure 7 gives an overview of the most important challenges for the calculation of ESs in octahedral first-row aqua-complexes, the presence of a degenerate GS and/or double excitations. The electron configuration is shown too, where we assumed that for all complexes the high-spin state is the most stable one. Remark that Mn^{2+} with the d^5 configuration has been omitted, as this complex has no spin-allowed d−d transitions.

First of all, whether the GS is degenerate or not is indicated in red or green, respectively. As can be seen, most of the octahedral TMCs have a degenerate GS, the only exceptions are V^{2+} and Ni^{2+}. On the one hand, configuration averaging, as is done in AOC, is, in principle, necessary to treat the degenerate microstates of the GS equally. On the other hand, the degeneracy is mostly elevated by Jahn−Teller (JT) effects,[52] which has been investigated for some of the complexes in our previous work.[5] This is in agreement with the results of Shee et al., who have recently put forward that in most TMCs, static correlation is rarely found in the GS.[53] Therefore, we also performed UDFT calculations, in which one of the degenerate microstates in the GS is selected. TDDFT, being a single reference technique, calculates the ESs based on this GS reference. In Figures 3 and 4, this microstate is indicated with a solid line. For the octahedral d^7 TMC, we arbitrarily chose one of the three microstates with maximal spin-projection corresponding to $^4T_{1g}(F)$ as the GS reference, namely a. The fact that TDDFT selects a specific microstate as reference from which excitations are determined has two consequences. First of all, the other two microstates belonging to $^4T_{1g}(F)$, b and c, are reached via single excitations. These single excitations are indicated with dashed lines. Second, only four of the six microstates corresponding to $^4T_{1g}(P)$ and $^4T_{2g}$ are reached via an excitation of a single electron. These are d, e, g, and h and are indicated with a dashed line. f and i can only be reached when two electrons are excited from the GS reference. These double excitations are indicated with a dotted line. This has been addressed in ref 10 as well. Microstate j corresponding to $^4A_{2g}$ is also a double ES. The behavior of the tetrahedral d^7 complexes shown in Figure 4 is different. All microstates corresponding to $^4T_2$ and $^4T_1(F)$, i.e., b−g, are single ESs, and all microstates corresponding to $^4T_1(P)$, i.e., h−j, are double ESs. Therefore, they are indicated with dashed and dotted lines, respectively.

It is widely known that, due to the adiabatic approximation, TDDFT is not capable of treating ESs with mainly double excitation character.[54] Let us consider the two situations studied before. In the case of a nondegenerate GS, as for example in Figure 4, there are three double excitations, as stated before. They correspond to the transfer of two e_g electrons to t_{2g} orbitals, leading to the $^4T_1(P)$ state. Interactions can occur between the single $^4T_1(F)$ and double $^4T_1(P)$ ESs, as visualized by the bending of both lines in the TS diagram. However, TDDFT is not capable of reproducing the double excitations and will only generate single ESs too high in energy as the interaction with the double ESs is lacking.[54] Now, consider the case of a degenerate GS as presented in Figure 3. According to the TS diagram, there is only one double ES state, $^4A_{2g}$, which does not have any ESs with matching symmetry with which it can interact. However, due to the fact that TDDFT selects a specific GS, also microstates f and i become double ESs. They have symmetry $^4T_{1g}$ or $^4T_{2g}$ and therefore, interactions with $^4T_{1g}(F)$ can occur.

In the following, we will divide the TMCs shown in Figure 7 in three categories, based on the degeneracy of the GS and the presence of double ESs, and compare the performance of LFDFT and TDDFT. We start with V^{2+} and Ni^{2+} with nondegenerate GSs. In this category, we will also consider tetrahedral d^7 complexes, as they play a central role in the search for a possible fingerprint for the ZIF nucleation process. After this, we study Sc^{2+}, Cr^{2+}, Fe^{2+}, and Cu^{2+}, which have a degenerate GS, but for which no double excitations are present. We conclude with the most difficult systems, Ti^{2+} and Co^{2+}, which have both a degenerate GS and the presence of double excitations. A proper description of the latter is also indispensable in order to unravel the nucleation process. Before we dive into this, we first discuss the computational details.

3. COMPUTATIONAL DETAILS

The AOC, UDFT, LFDFT, and unrestricted TDDFT calculations were performed with Amsterdam modeling suite (AMS).[55] As in this work we only focus on isolated complexes and not on the Co-ZIF-67 material nor on the metal−organic pool, we only performed cluster calculations. The TZ2P$^+$ basis set, with extra d-Slater type orbitals (STO), was applied for the TMs, and the TZ2P basis set was used for the other elements. In analogy to our previous work,[5] we have chosen to apply the B3LYP-D3 functional.[56,57] Grimme D3 dispersion corrections have also been added.[58] The calculations performed in this work use this level of theory unless explicitly stated otherwise. As it is well-known that TDDFT results can strongly depend on the used functional,[8] two other functionals have also been tested for $[Co(H_2O)_6]^{2+}$, namely, PBE0[59] and ωB97,[60] as they are known to perform good for the description of TMCs and are available in AMS.[61,62] Methanol has been included as a solvent using COSMO.[63] Recently, Radoń et al. stated that the inclusion of the second solvation shell is essential to correctly determine the ESs of octahedral aqua-complexes.[14] However, in this work, the situation is more

https://doi.org/10.1021/acs.inorgchem.3c01355
Inorg. Chem. XXXX, XXX, XXX−XXX

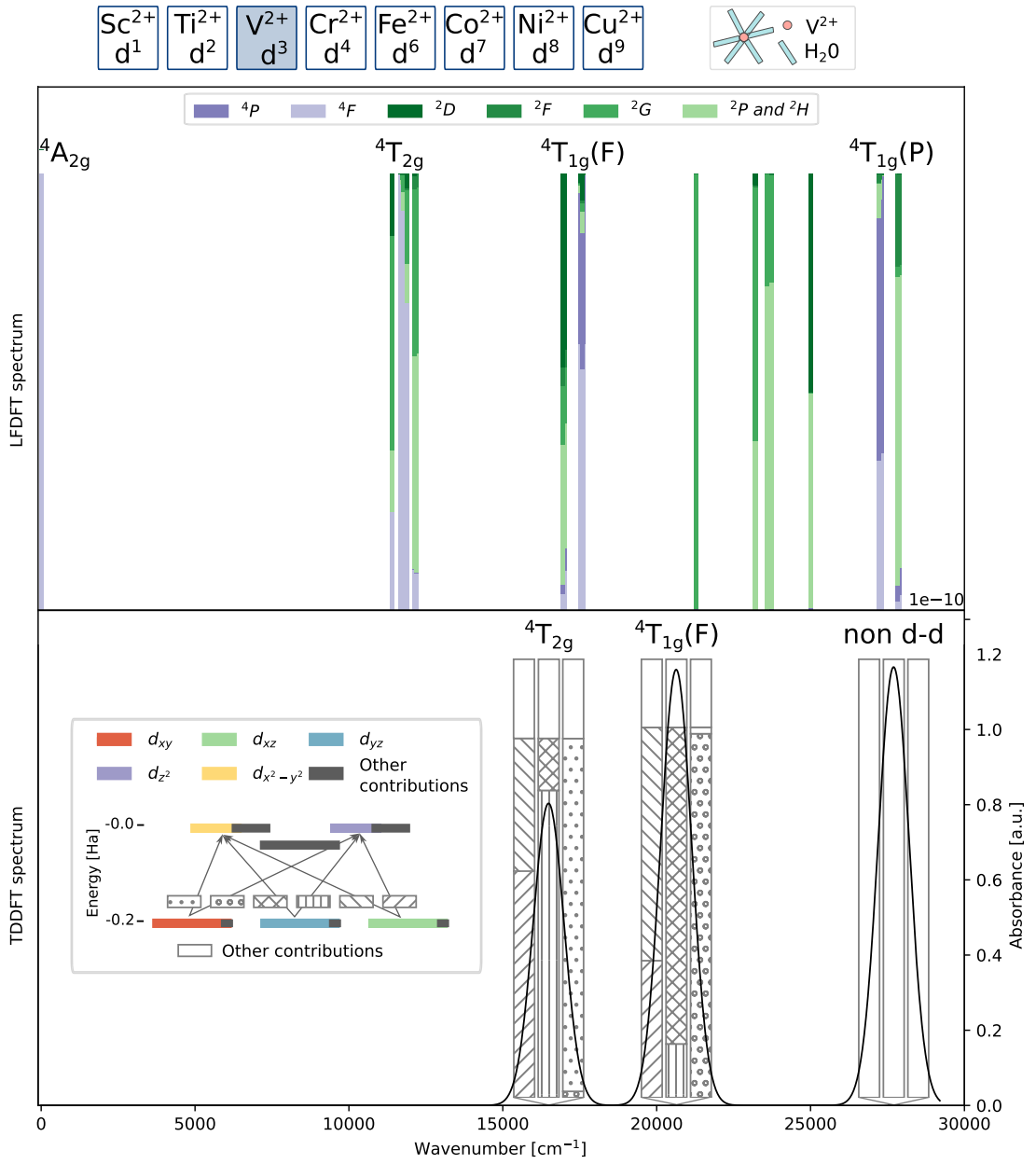

Figure 8. LFDFT (top) and TDDFT (bottom) spectrum of $[V(H_2O)_6]^{2+}$ with D_{2h} symmetry. The vertical bars in the LFDFT spectrum indicate the contribution of each microstate. The degeneracy is not displayed. In the TDDFT spectrum, the vertical bars show the excitations with mainly d−d character, whereby the largest contributions are denoted. The legend for the different hatch types is given in the inset in which the α d-orbital splitting obtained via UDFT is presented. The black curve represents the convoluted absorption spectrum, for which the axis is presented on the right.

complicated, as the complexes are situated in a methanol environment to mimic the experimental conditions valid in the formation of ZIFs. A full study of the influence of the solvation environment on the ESs of the TMCs is beyond the scope of this work, as our focus is on the development of a qualitative fingerprint to follow the nucleation process of ZIFs. Scalar relativistic effects were taken into account using the ZORA formalism.[64−66] Geometry optimizations were performed using UDFT. We checked that all computed internal normal modes of the optimized structures show positive frequencies, ensuring that the geometries represent minima of the GS potential energy surface. The optimized coordinates of all complexes studied in this work are given in section 3 of the Supporting Information. The symmetry of the complexes has been determined by GaussView 5.0.[67] Although they do not have perfect octahedral and tetrahedral symmetry, we will, for the sake of simplicity, use the O_h and T_d symmetry labels to designate the states. In the TDDFT calculations, the lowest 30 excitations have been determined. We convoluted the simulated TDDFT spectra with a Gaussian envelope with a standard deviation of 500 cm^{-1} to simulate the Franck−Condon width of spectra. TDDFT can be performed with or without the symmetry keyword. The main advantage of adding the keyword is that it allows one to determine the symmetry of the ESs, which, in addition to their main contributions, can be helpful for labeling. The biggest disadvantage is that, when symmetry is invoked, the oscillator strength is, per definition, zero. Spin-forbidden ESs can in principle be calculated using spin-flip (SF)-TDDFT.[8,68,69] However, these transitions are composed of many small contributions, making it difficult to label them. Furthermore, as they are spin-forbidden, they are much less intense than the excitations calculated via regular TDDFT. Therefore, we do not further discuss spin-forbidden excitations. Spin orbit coupling (SOC) was included in the LFDFT calculations. Although the degeneracy of the states in the subsequent

https://doi.org/10.1021/acs.inorgchem.3c01355
Inorg. Chem. XXXX, XXX, XXX−XXX

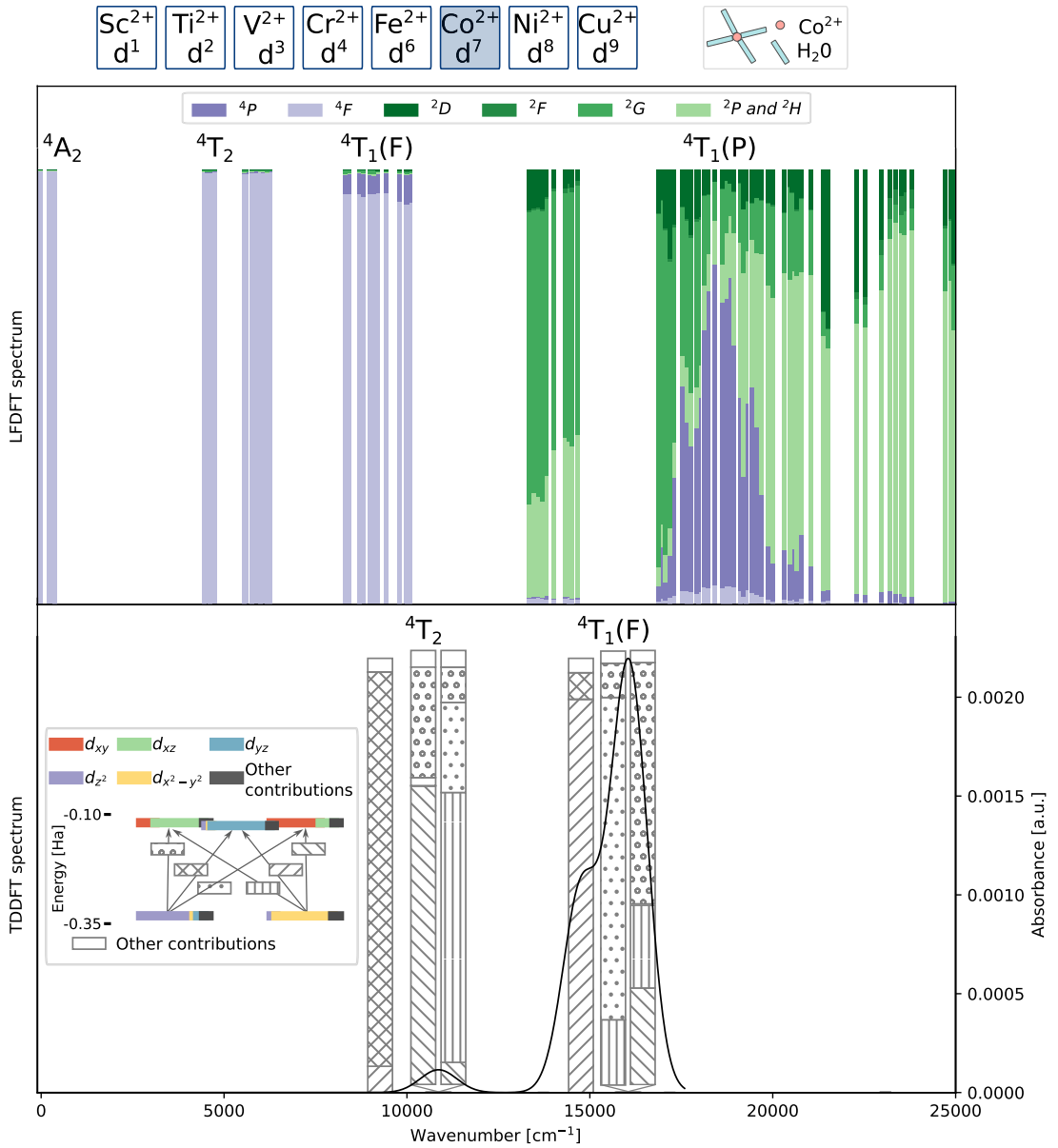

Figure 9. LFDFT (top) and TDDFT (bottom) spectrum of $[Co(H_2O)_4]^{2+}$. The vertical bars in the LFDFT spectrum indicate the contribution of each microstate. The degeneracy is not displayed. In the TDDFT spectrum, the vertical bars show the excitations with mainly d−d character, whereby the largest contributions are denoted. The legend for the different hatch types is given in the inset, in which the β d-orbital splitting obtained via UDFT is presented. The black curve represents the convoluted absorption spectrum, for which the axis is presented on the right.

LFDFT spectra is not shown, this information has been used to group the microstates and to characterize them with labels according to the TS diagrams.

The AILFT calculations are parametrized via N-electron valence perturbation theory (NEVPT2) using ORCA.[70,71] In order to estimate the effect of dynamical correlation, we compared the results with AILFT calculations starting from a CASSCF(7,5) reference, which does not capture these correlation effects. These calculations are computationally more expensive than the DFT-based techniques and have been performed using a minimal active space as it was found in refs 6 and 7 that this is sufficient for SORCI and multireference calculations, respectively. Although it is expected that the effect of increasing the d-orbital space is small for TMCs with an oxidation state of +2, additional investigations are needed to further test the influence of the active space size. The def2-TZVP basis set has been used and the methanol solvent has been included via the conductor-like polarizable continuum model (C-PCM).[72]

We note that the complexes studied in this work are positively charged. This charge can be counterbalanced by the NO_3^- ligands surrounding the TMCs. In addition, it is possible that some of the ligands get deprotonated. However, this depends on the pH of the solution. Setting up models that account for these complexities of the molecular environment would be very complex and is beyond the scope of this study.

4. RESULTS AND DISCUSSION

4.1. First-Row Aqua-Complexes. *4.1.1. Nondegenerate GS but Double Excitations: $[V(H_2O)_6]^{2+}$, $[Ni(H_2O)_6]^{2+}$, and Tetrahedral $[Co(H_2O)_4]^{2+}$.* $[V(H_2O)_6]^{2+}$ and $[Ni(H_2O)_6]^{2+}$ complexes have a d^3 and d^8 configuration, respectively, and thus nondegenerate GSs. Stable structures with D_{2h}, T_h, and S_6 symmetry were obtained. For the V^{2+} complexes, the d-orbital splitting is shown in Figure S3. The LFDFT and TDDFT spectra are shown in Figures 8, S4, and S5. Ni^{2+} complexes

https://doi.org/10.1021/acs.inorgchem.3c01355
Inorg. Chem. XXXX, XXX, XXX−XXX

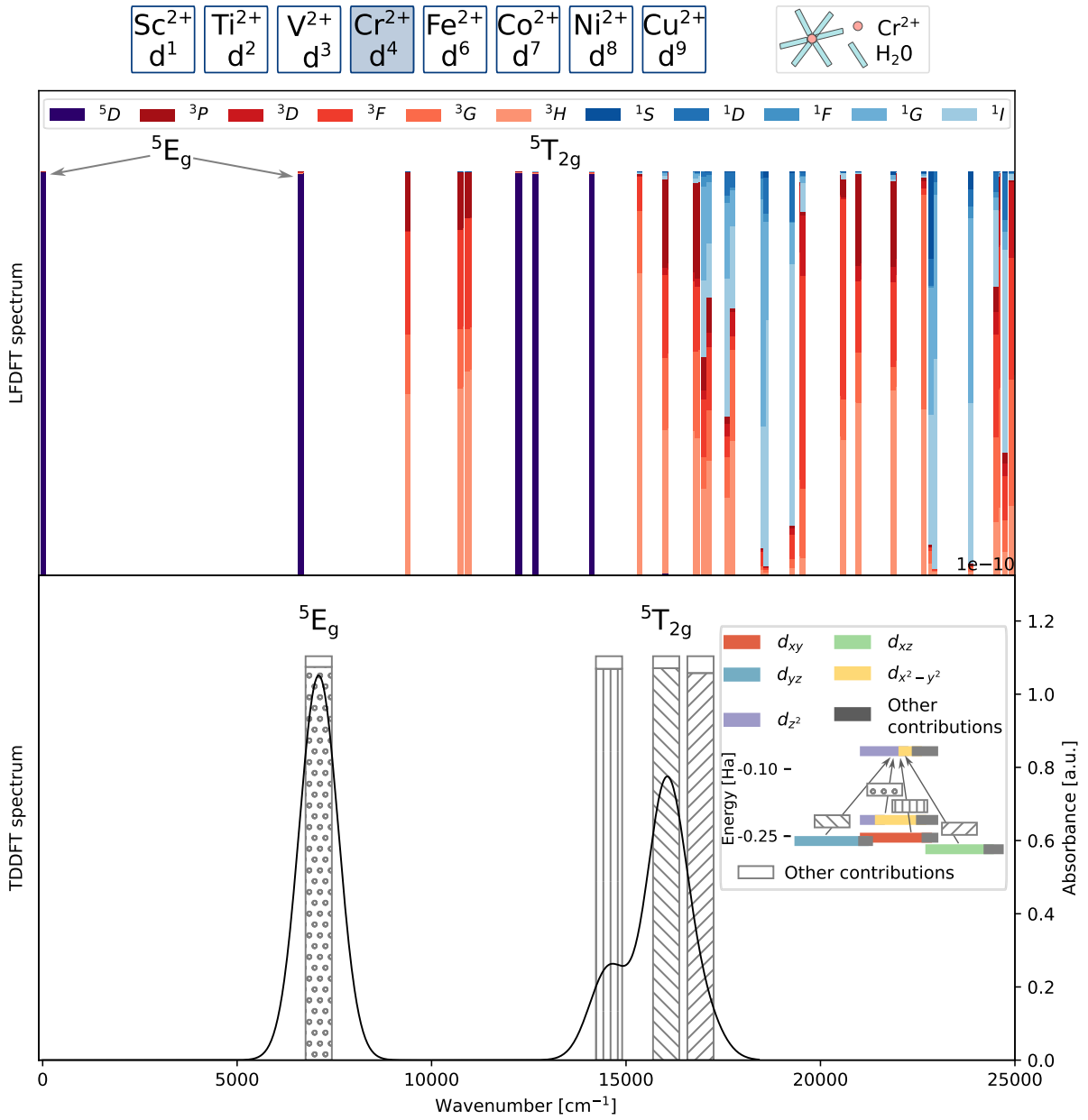

Figure 10. LFDFT (top) and TDDFT (bottom) spectrum of $[Cr(H_2O)_6]^{2+}$ with D_{2h} symmetry. The vertical bars in the LFDFT spectrum indicate the contribution of each microstate. The degeneracy is not displayed. In the TDDFT spectrum, the vertical bars show the excitations with mainly d−d character, whereby the largest contributions are denoted. The legend for the different hatch types is given in the inset in which the α d-orbital splitting obtained via UDFT is presented. The black curve represents the convoluted absorption spectrum, for which the axis is presented on the right.

have similar results, as presented in Figures S6−S9. As equivalent conclusions can be drawn for the different symmetries, we discuss only the complexes with D_{2h} symmetry in detail. The only difference from the other complexes is that the peaks in the LFDFT spectra are much broader for the S_6 complex. Also, as the S_6 complexes have the least symmetry, the oscillator strengths calculated by TDDFT are a little bit larger, although they remain very small.

First, we take a look at $[V(H_2O)_6]^{2+}$ and examine the LFDFT results in the top pane of Figure 8. The microstates are plotted as vertical bars, of which the colors represent their contributions, the quartet states are shown in purple and the doublet states in green. As stated in section 3, the labeling of the microstates according to the TS diagrams is based on their contributions and degeneracy. First of all, at around 0 cm^{-1}, the nondegenerate $^4A_{2g}$ GS is situated, which is purely ^4F. Furthermore, the second region with quartet states is situated around 11750 cm^{-1}, contains large portions of ^4F and corresponds to the $^4T_{2g}$ state. Remark that some contributions of doublet states occur to. The third quartet region at 17600 cm^{-1} contains significant parts from both ^4F and ^4P. The same holds for the band at around 27250 cm^{-1}. They are labeled as $^4T_{1g}(F)$ and $^4T_{1g}(P)$, respectively. As can be seen in the TS diagram shown in Figure 4, $^4T_{1g}(F)$ and $^4T_{1g}(P)$ correspond to single and double excitation, respectively. They have the same symmetry and mixing is observed in the LFDFT spectrum. In between the previously stated bands doublet contributions are present which will not be analyzed further.

https://doi.org/10.1021/acs.inorgchem.3c01355
Inorg. Chem. XXXX, XXX, XXX−XXX

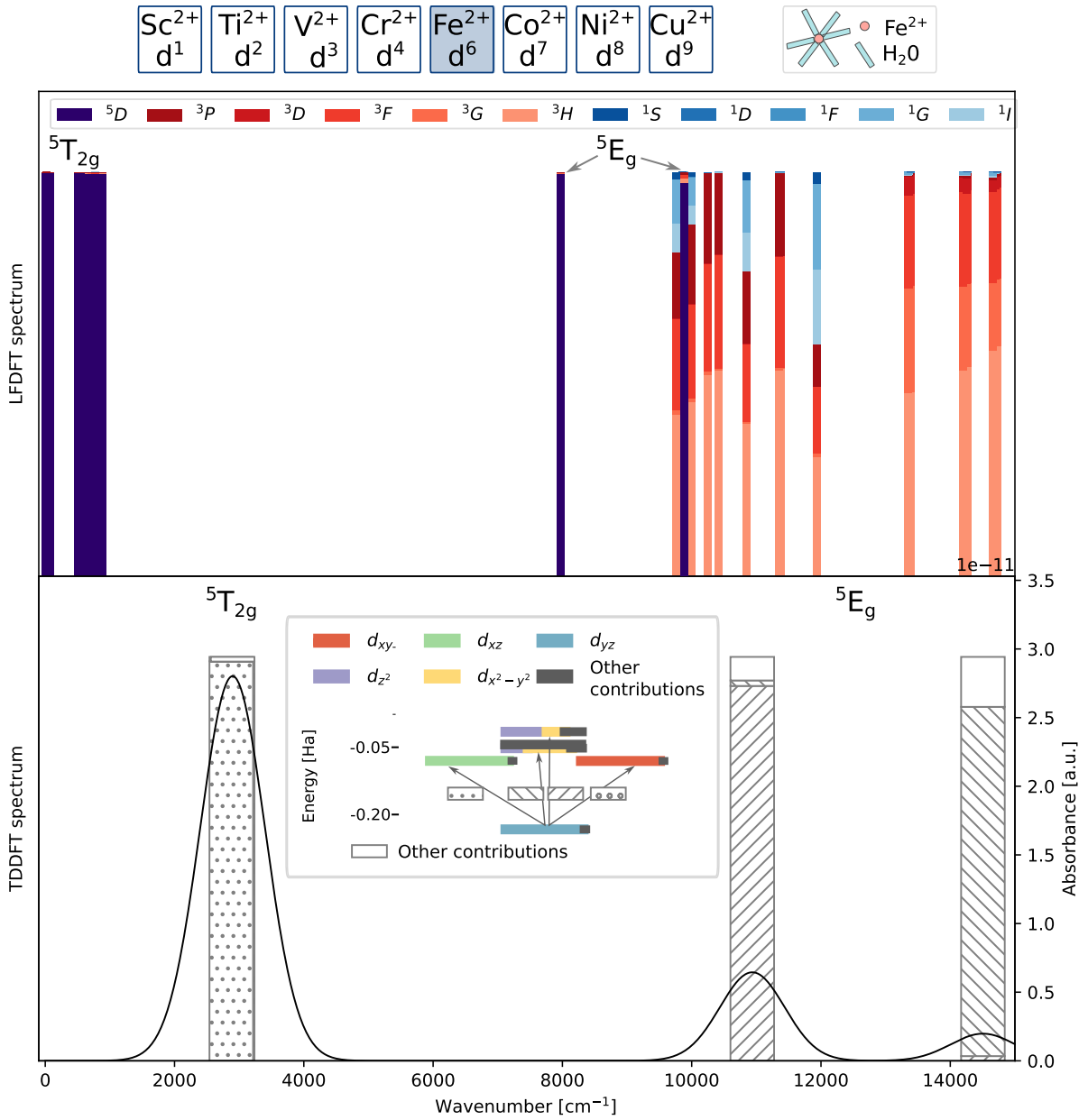

Figure 11. LFDFT (top) and TDDFT (bottom) spectrum of $[Fe(H_2O)_6]^{2+}$ with D_{2h} symmetry. The vertical bars in the LFDFT spectrum indicate the contribution of each microstate. The degeneracy is not displayed. In the TDDFT spectrum, the vertical bars show the excitations with mainly d−d character, whereby the largest contributions are denoted. The legend for the different hatch types is given in the inset in which the β d-orbital splitting obtained via UDFT is presented. The black curve represents the convoluted absorption spectrum, for which the axis is presented on the right.

Now, let us inspect the TDDFT results in the bottom pane of Figure 8. The black curve represents the convoluted absorption spectrum, whereas the vertical bars positioned at the excitation energies are hatched according to the main contributions present in the ES. The different hatch styles are introduced in the inset showing the d-orbital splitting obtained by UDFT. There are six excitations with mainly d−d character, grouped in two clusters of three states each. Every ES is attributed to a transition from a t_{2g} to an e_g orbital. They correspond to the microstates b−g in Figure 4 and the clusters can be labeled as $^4T_{2g}$ and $^4T_{1g}(F)$, respectively. Note the presence of an ES in the region where double excited state $^4T_{1g}(P)$ in the LFDFT spectrum occurs. As it has no d−d character, it does not correspond to $^4T_{1g}(P)$. Indeed, TDDFT is not capable of determining double excitations. Finally remark the very small oscillator strengths for all the ESs.

In our previous work, we observed that the gap between occupied and unoccupied orbitals is overestimated in UDFT compared to AOC.[5] Although the gap is ca. 43000 cm^{-1} versus 11000 cm^{-1} for $[V(H_2O)_6]^{2+}$, the qualitative pictures of the ESs computed by LFDFT and TDDFT agree rather well apart from a shift to higher energies of only 3000−4700 cm^{-1}. The overestimation of the excitation energy of $^4T_{1g}(F)$ can be explained by the fact that the double excited $^4T_{1g}(P)$ is missing in TDDFT as explained in section 2.2.

The results are very similar for the Ni^{2+} complexes. Triplet and singlet states are indicated with shades of red and blue, respectively. We observe that there is little mixing between the

https://doi.org/10.1021/acs.inorgchem.3c01355
Inorg. Chem. XXXX, XXX, XXX−XXX

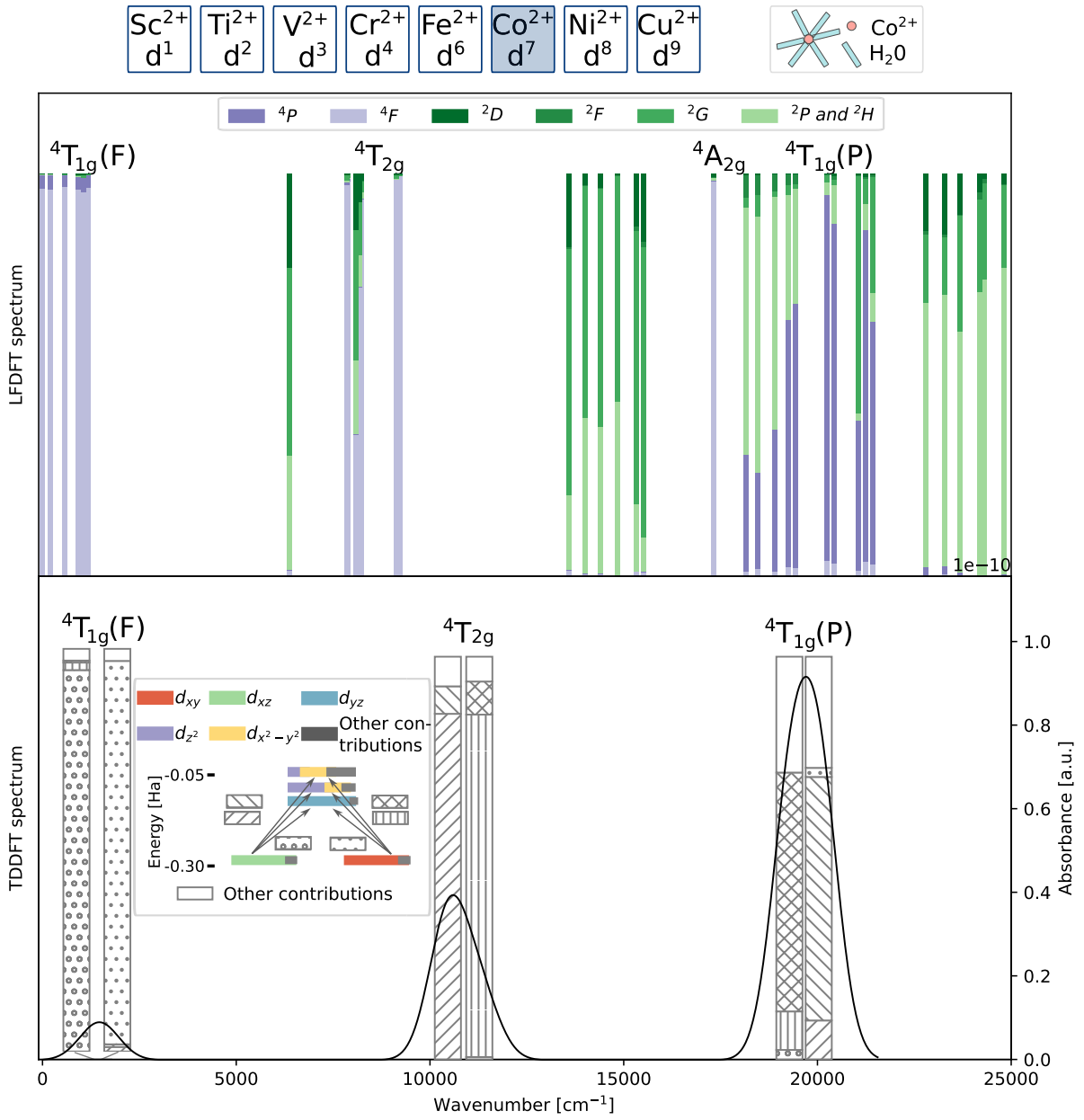

Figure 12. LFDFT (top) and TDDFT (bottom) spectrum of $[Co(H_2O)_6]^{2+}$ with D_{2h} symmetry. The vertical bars in the LFDFT spectrum indicate the contribution of each microstate. The degeneracy is not displayed. In the TDDFT spectrum, the vertical bars show the excitations with mainly d−d character, whereby the largest contributions are denoted. The legend for the different hatch types is given in the inset in which the β d-orbital splitting obtained via UDFT is presented. The black curve represents the convoluted absorption spectrum, for which the axis is presented on the right.

single and double excited $^3T_{1g}$ states. In the TDDFT spectrum, there are again six d−d ESs, grouped into two peaks, $^4T_{2g}$ and $^4T_{1g}(F)$, respectively.

Based on the results of these complexes with nondegenerate GSs, we can provisionally conclude that, even though the excitation spectrum contains double ESs and the d-orbital splitting between the occupied and unoccupied orbitals is overestimated by UDFT compared to AOC, TDDFT, and LFDFT yield qualitatively similar results for the d−d excitations. However, one must keep in mind that double excitations are not retrieved by TDDFT and one must verify the character of the ES to confirm whether it is a d−d transition or not.

Before investigating the performance of LFDFT and TDDFT for systems with degenerate GSs, we first consider tetrahedral $[Co(H_2O)_4]^{2+}$, as similar four-coordinated complexes with aqua and 2-mIm ligands will play an important role in the second part of this work. As can be seen in the TS diagram shown in Figure 4, these complexes have, as $[V(H_2O)_6]^{2+}$ and $[Ni(H_2O)_6]^{2+}$, a nondegenerate GS and contain double excitations. $[Co(H_2O)_4]^{2+}$ has been subject of our preceding work, in which an optimal structure has been obtained.[5] The d-orbital splitting is shown in Figure S10 and the LFDFT and TDDFT spectra in Figure 9. In the LFDFT spectrum, we can clearly distinguish the $^4A_2$ GS and $^4T_2$ and $^4T_1(F)$ single excitations, which all have almost exclusively ^4F contributions. The $^4T_1(P)$ band corresponding to double

https://doi.org/10.1021/acs.inorgchem.3c01355
Inorg. Chem. XXXX, XXX, XXX−XXX

excitation is rather broad. Moreover, there is very little mixing between the $^4T_1(F)$ single and $^4T_1(P)$ double excitations. When investigating the TDDFT spectrum, we first of all remark the much larger oscillator strengths observed in the TDDFT results, which is in agreement with our expectations for these noncentrosymmetric tetrahedral complexes. This information can not be obtained from LFDFT calculations. Furthermore, there are again six ESs in which an electron is transferred from an e orbital to a t_2 orbital and which correspond to transitions to the microstates b−g in Figure 4. These single ESs are grouped in two clusters and are labeled $^4T_2$ and $^4T_1$. As there is a significant shift between the LFDFT and TDDFT results, we also tested the performance of PBE0 and ωB97, for which the spectra are shifted toward larger and smaller wavelengths with respect to B3LYP, respectively, as shown in Figures S11−S13. The excitation energies strongly depend on the chosen functional, as shifts up to 3700 cm^{-1} are observed.

As such, we conclude that also for tetrahedral complexes with nondegenerate GSs, the picture of d−d excitations obtained from LFDFT and TDDFT is qualitatively similar. Moreover, both techniques give Supporting Information, whereas LFDFT is capable of describing double excitations and TDDFT yields oscillator strengths. Nevertheless, the exact position of the ESs obtained from TDDFT strongly depend on the functional and differ from the LFDFT results. Therefore, a quantitative comparison with experimental data will be given for the complexes studied in the second part of this work.

4.1.2. Degenerate GS but No Double Excitations: $[Sc(H_2O)_6]^{2+}$, $[Cr(H_2O)_6]^{2+}$, $[Fe(H_2O)_6]^{2+}$, and $[Cu(H_2O)_6]^{2+}$. Now, we look into the more complicated complexes which have a degenerate GS, but do not contain double excitations. We found stable $[Cr(H_2O)_6]^{2+}$ and $[Fe(H_2O)_6]^{2+}$ complexes with D_{2h} symmetry. This is the highest possible symmetry, as the GS is degenerate. The d-orbital splitting is shown in Figures S14 and S15, respectively and the LFDFT and TDDFT spectra in Figures 10 and 11. A large difference between the Cr^{2+} and Fe^{2+} complexes is that the e_g set is degenerate for the former, whereas it is the t_{2g} set for the latter, which corresponds to strong and weak JT distortions, respectively. This is also reflected in the LFDFT spectra, as the spread in the GS term, being ^5E_g and $^5T_{2g}$, is much larger for the former than for the latter. The same observation is made for the TDDFT spectra. The first peak is located at energies larger for $[Cr(H_2O)_6]^{2+}$ than for $[Fe(H_2O)_6]^{2+}$ and corresponds to $e_g \rightarrow e_g$ and two $t_{2g} \rightarrow t_{2g}$ transitions, respectively. The other quintet states, $^5T_{2g}$ for Cr^{2+} and ^5E_g for Fe^{2+}, are situated at higher energies. There are respectively three and two peaks in the LFDFT spectrum that clearly agree with the three $t_{2g} \rightarrow e_g$ and two $e_g \rightarrow t_{2g}$ excitations in the TDDFT spectrum. Finally, we note that there is no mixing between the triplet or singlet contributions and the quintet states. From these case studies, we can conclude that the degeneracy of the GS poses no extra challenges for the calculation of d−d excitations via LFDFT and TDDFT.

As for $[Sc(H_2O)_6]^{2+}$ some other orbitals are situated in between the d-orbitals in the AOC results shown in Figure S16, LFDFT can not be applied. Furthermore, the most common oxidation state of Sc^{2+} is +3. For $[Cu(H_2O)_6]^{2+}$ too, some problems have been encountered as no stable structures have been found in the methanol solvent environment. Therefore, we will not elaborate further on these complexes.

4.1.3. Degenerate GS and Double Excitations: $[Ti(H_2O)_6]^{2+}$ and $[Co(H_2O)_6]^{2+}$. A stable $[Co(H_2O)_6]^{2+}$ structure with D_{2h} symmetry has been obtained previously, but is reoriented such that the smallest metal-bond distance is directed along the z-direction.[5] For completeness, the d-orbital splitting, extensively discussed in ref 5, is shown in the left pane of Figure S17. The spectra are presented in Figure 12. In order of increasing energy, we can clearly discern the $^4T_{1g}(F)$ GS, single excited $^4T_{2g}$, double excited $^4A_{2g}$, and single excited $^4T_{1g}(P)$ in the LFDFT spectrum. Remark that mixing between the single and double excitations is limited. For the TDDFT spectrum, six ESs occur, which correspond to transitions from the GS to the microstates b−e, g, and h, as shown in Figure 3. They are grouped in three clusters of two ESs each. The first two are excitations in between the t_{2g} orbital set, corresponding to the microstates b and c, reached via a single excitation from the GS reference a. These two ESs can thus be labeled as $^4T_{1g}(F)$. For the other four excitations, an electron is excited from a t_{2g} to an e_g orbital, which are thus labeled as $^4T_{2g}$ and $^4T_{1g}(P)$. We also tested the performance of the PBE0 and ωB97 functionals for this complex as shown in Figures S18−S20. The position of $^4T_{1g}(P)$ is shifted to larger/smaller wavelengths compared to the B3LYP results for PBE0 and ωB97, respectively. The functional dependence is less pronounced than for $[Co(H_2O)_4]^{2+}$, but shifts up to 1900 cm^{-1} are still observed. A comparison with the experimental results of Filez et al. and other literature data is given in the next section.

In ref 5, we also found a stable structure with S_6 symmetry, which has been reoriented such that the ligands are oriented as much as possible toward the coordinate axes. The results are shown in the right pane of Figures S17 and S21. The LFDFT spectra for the D_{2h} and S_6 complexes are in good agreement. However, discrepancies are observed between the TDDFT spectra. Only one ES is corresponding to $^4T_{1g}$, which is at much larger energies in the S_6 complex than in the D_{2h} system. Furthermore, one can not distinguish the $^4T_{2g}$ and $^4T_{1g}(P)$ states. An identical behavior has been observed for d^2 $[V(H_2O)_6]^{3+}$ complexes presented in Figures S22−S24.

Unfortunately, the AOC results show that other orbitals are situated in between the d-orbitals for $[Ti(H_2O)_6]^{2+}$ as shown in Figure S25. Hence, this complex will not be studied further.

From this case study of octahedral TMCs with first-row TMs and aqua ligands, extended with tetrahedral Co^{2+} aqua-complexes, we can conclude that LFDFT and TDDFT yield qualitative similar results, which are complementary to each other. Whereas LFDFT is capable of describing double excitations, TDDFT allows one to determine oscillator strengths. The overestimation of the gap between the occupied and unoccupied orbitals by UDFT compared to AOC is not reflected in the excitation spectra. Even the d−d excitations in challenging systems, with a degenerate GS and double excitations, can be described qualitatively correctly by both techniques. However, care must be taken for complexes with degenerate GSs and double excitations possessing S_6 symmetry, for which only LFDFT yields reasonable results. Furthermore, as for some ESs, the excitation energy is different for the TDDFT and LFDFT results, a comparison with experimental data is necessary. This will be addressed in the next section, in which we apply both LFDFT and TDDFT to TMCs relevant for the nucleation of ZIFs. The results of the octahedral Co^{2+} complexes with aqua ligands presented in this section are complemented with spectra of tetrahedral Co^{2+} complexes with aqua and/or 2-mIm ligands as indicated in Figure 1. Furthermore, we will compare our computational

https://doi.org/10.1021/acs.inorgchem.3c01355
Inorg. Chem. XXXX, XXX, XXX−XXX

results for these systems with experimental data and we will briefly investigate the performance of AILFT.

4.2. Spectroscopic Fingerprint for the Nucleation of Co-ZIF-67. As stated in the Introduction, the mixture obtained after mixing $Co(NO_3)_2{\cdot}6H_2O$ and 2-mIm mainly consists of the complexes indicated in gray in Figure 1 according to ref.[4] The experimental UV−vis spectrum of the mixture is shown in blue in Figure 13. A linear combination fit (LCF) presented

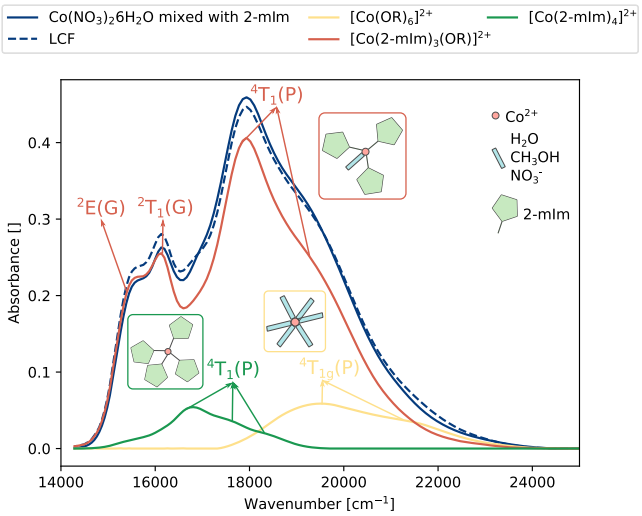

Figure 13. Experimental absorption spectra in the visible range of the electromagnetic spectrum after $Co(NO_3)_2{\cdot}6H_2O$-2-mIm mixing (blue). A LCF (blue, dotted) deconvolutes the spectrum in $[Co(OR)_6]^{2+}$ (yellow), $[Co(2\text{-mIm})_3(OR)]^{2+}$ (red), and $[Co(2\text{-mIm})_4]^{2+}$ (green) constituents. Figure adapted from ref 4 with permission of Elsevier, Copyright 2021.

with a dashed line deconvolutes the spectrum in three main contributions. The yellow curve corresponds to $[Co(OR)_6]^{2+}$ complexes, whereby OR can be water, methanol, or NO_3^-. Red indicates $[Co(2\text{-mIm})_3(OR)]^{2+}$ and the green curve has been identified as $[Co(2\text{-mIm})_4]^{2+}$. In the following, we will investigate each structure separately. Note that excitations below 14000 cm^{-1} are not measured as this region is situated in the near-infrared lying outside the scope of the work presented in ref.[4]

4.2.1. [Co(2-mIm)$_4$]$^{2+}$. The $[Co(2\text{-mIm})_4]^{2+}$ complex indicated in green in Figure 13 is characterized by the $^4T_1(P)$ state observed as the three spin−orbit split subpeaks situated at 16667, 17637, and 18315 cm^{-1}. This is in agreement with Banci et al., who used the angular overlap method to state that, for general tetrahedral Co^{2+} complexes, the $^4T_1(P)$ state is situated in the region between 13500 and 19500 cm^{-1}.[73] Furthermore, he showed that these complexes have two additional ESs at lower energies, namely $^4T_2$ and $^4T_1(F)$. The latter lies in the region between 5000 and 11000 cm^{-1}, whereas the former is situated below 5000 cm^{-1} and is therefore difficult to detect.[73] As these states are not situated in the range of UV−vis, they are not observed in Figure 13. An overview of ESs in tetrahedral Co^{2+} complexes can be found in ref 74.

We performed LFDFT and TDDFT calculations for this complex. Note that in our calculations we used 1,2-dimethylimidazole (1,2-dmIm) instead of 2-mIm to prevent dimerization and to exclusively study the initial change in the symmetry and coordination of Co^{2+}. The geometrical structure is shown in the left pane of Figure 14. The d-orbital splitting is shown in Figure S26. We compare the LFDFT and TDDFT

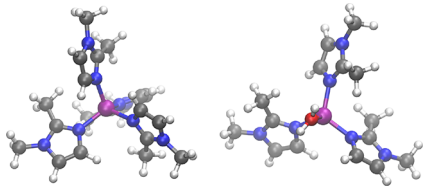

Figure 14. Visualization of the geometrical structure of $[Co(1,2\text{-dmIm})_4]^{2+}$ (left) and $[Co(1,2\text{-dmIm})_3(H_2O)]^{2+}$ (right). Carbon, cobalt, hydrogen, nitrogen, and oxygen are indicated in gray, purple, light gray, blue, and red, respectively.

spectra presented in Figure 15 with these of $[Co(H_2O)_4]^{2+}$ in Figure 9 in order to estimate the influence of changing the ligands from aqua to 2-mIm. First of all, we note that the oscillator strengths in the TDDFT results are four times larger than those of $[Co(H_2O)_4]^{2+}$. Furthermore, there are some minor shifts in the ESs, resulting in a more pronounced left shoulder of the second band, but the overall picture remains unaltered. $^4T_2$ is situated around 10000 cm^{-1}, whereas $^4T_1(F)$ is located around 15000 cm^{-1}. Compared to the results of Banci et al., we must conclude that the spectra are strongly blue-shifted over around 5000 cm^{-1}. This is maybe due to our choice of functional. Indeed, as stated previously, the specific position of the peak as calculated by TDDFT strongly depends on the used functional. As $^4T_1(P)$ is a double excitation, it is not reachable by TDDFT. The microstates in the LFDFT spectra are no longer present in clusters, but they are more spread-out, making it difficult to determine the energies of the states. This is due to the fact that the imidazole ligands are less compact than the aqua ligands. We can roughly say that the $^4T_2$ state is located between 5000 and 8000 cm^{-1} and the $^4T_1(F)$ state lies between 9000 and 12000 cm^{-1}, which is in agreement with the results of Banci et al. The double excited $^4T_1(P)$ state is located at around 17500 cm^{-1}, in accordance with the results of Filez et al. However, as the bands are rather spread-out, very specific conclusions can not be drawn.

As the LFDFT spectrum of the tetrahedral complex with 1,2-dmIm ligands is rather diffuse, we performed AILFT-(NEVPT2) calculations too. The results are shown in Figure 16. Contrary to the LFDFT spectra, shown in the top pane of Figure 15, the states are grouped together. Comparison to the TDDFT spectrum shown in the bottom pane of Figure 15 reveals that $^4T_2$ and $^4T_1(F)$ are situated at much smaller energies with a shift of more than 5000 cm^{-1}, which is in good agreement with the findings of Banci et al. discussed in section 4.2.1. The double excited $^4T_1(P)$ state is situated at larger energies compared to the experimental spectrum shown in Figure 13 and the results of Banci et al.

4.2.2. [Co(2-mIm)$_3$(OR)]$^{2+}$. The following d−d excitations are discerned in the spectrum of $[Co(2\text{-mIm})_3(OR)]^{2+}$ indicated in red in Figure 13. First, two doublet ESs are observed: $^2E(G)$ at 15408 cm^{-1} and $^2T_1(G)$ at 16155 cm^{-1}. These spin-forbidden bands are the most narrow ones in the spectrum, which is in line with our expectations. Because these states correspond to the $t_2^3e^4$ configuration, as shown in Figure 4, it is also possible that some broadening occurs due to JT distortions. At 17825 and 19268 cm^{-1}, the double excited $^4T_1(P)$ state is situated. This spectrum is clearly different from that of $[Co(2\text{-mIm})_4]^{2+}$.

https://doi.org/10.1021/acs.inorgchem.3c01355
Inorg. Chem. XXXX, XXX, XXX−XXX

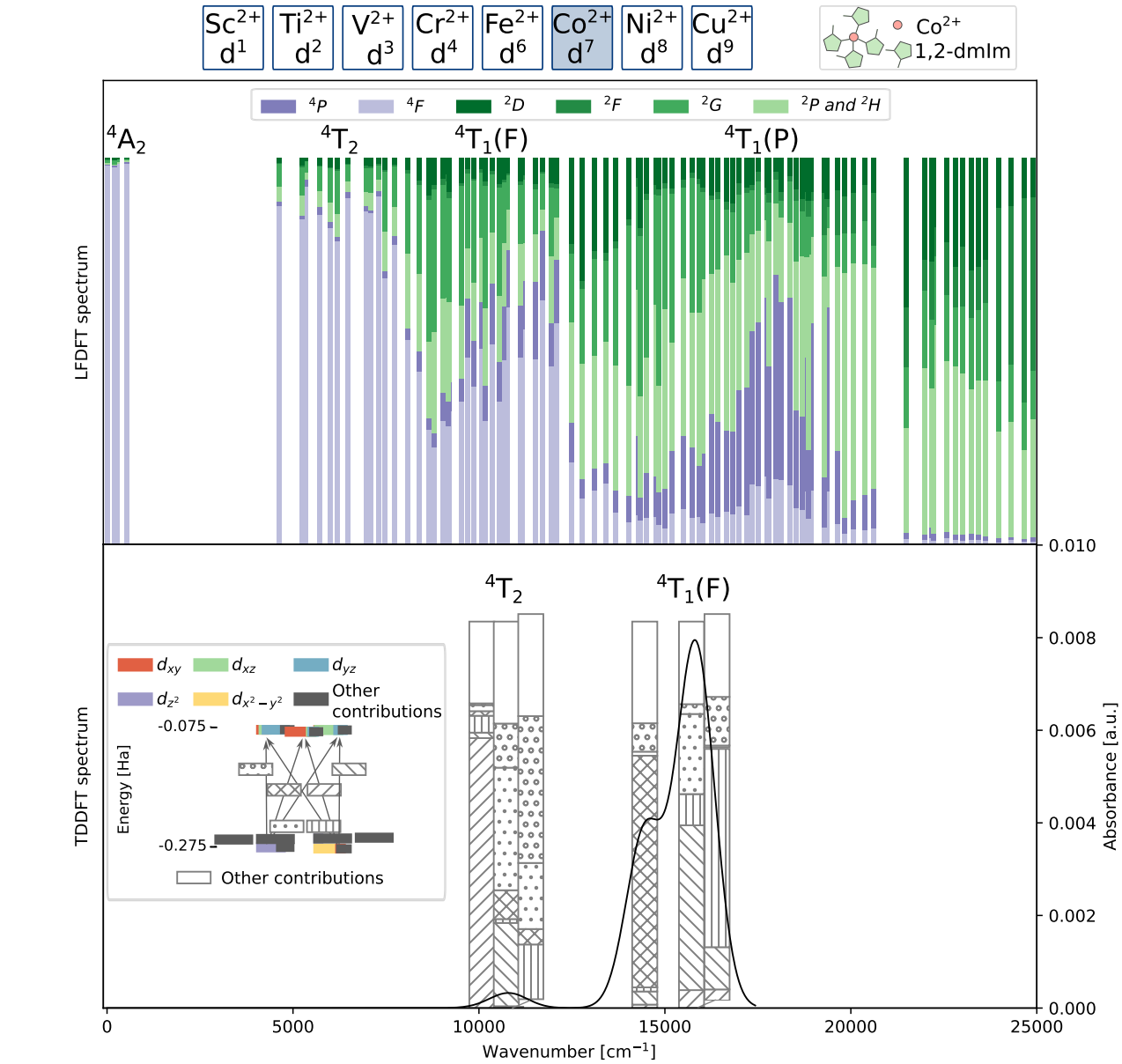

Figure 15. LFDFT (top) and TDDFT (bottom) spectrum of $[Co(1,2\text{-dmIm})_4]^{2+}$. The vertical bars in the LFDFT spectrum indicate the contribution of each microstate. The degeneracy is not displayed. In the TDDFT spectrum, the vertical bars show the excitations with mainly d−d character, whereby the largest contributions are denoted. The legend for the different hatch types is given in the inset in which the β d-orbital splitting obtained via UDFT is presented. The black curve represents the convoluted absorption spectrum, for which the axis is presented on the right.

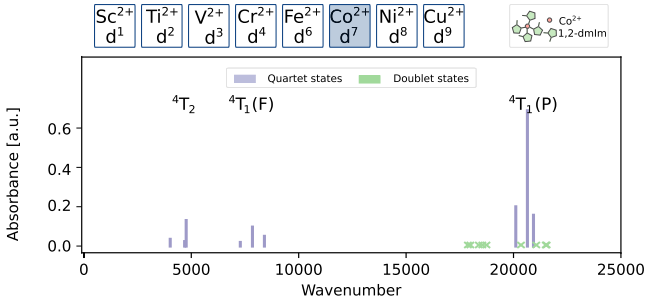

Figure 16. AILFT(NEVPT2) spectrum of $[Co(1,2\text{-dmIm})_4]^{2+}$. Quartet states are indicated in purple and their oscillator strength is presented by the height of the bar. The spin-forbidden doublet states are indicated with green crosses and have zero oscillator strength.

The geometrical structure of $[Co(1,2\text{-dmIm})_3(H_2O)]^{2+}$ is shown in the right pane of Figure 14. The splitting of the d-orbitals is shown in Figure S27 and the LFDFT and TDDFT spectra in Figure 17. We do not observe large differences concerning the d−d transitions corresponding with single excitations obtained via TDDFT between $[Co(1,2\text{-dmIm})_3(H_2O)]^{2+}$ and $[Co(1,2\text{-dmIm})_4]^{2+}$. We only note that there is no shoulder in the second band for the former complex. The four ESs identified in the experimental spectrum are not reachable by TDDFT as they are SF or double excitations. The LFDFT spectrum is even more diffuse than for the previous complex, making it impossible to draw conclusions from it. As the large differences between the tetrahedral Co^{2+} complexes found by Filez et al. are not observed by TDDFT, we conclude that more advanced techniques are needed, which are more precise and capable

https://doi.org/10.1021/acs.inorgchem.3c01355
Inorg. Chem. XXXX, XXX, XXX−XXX

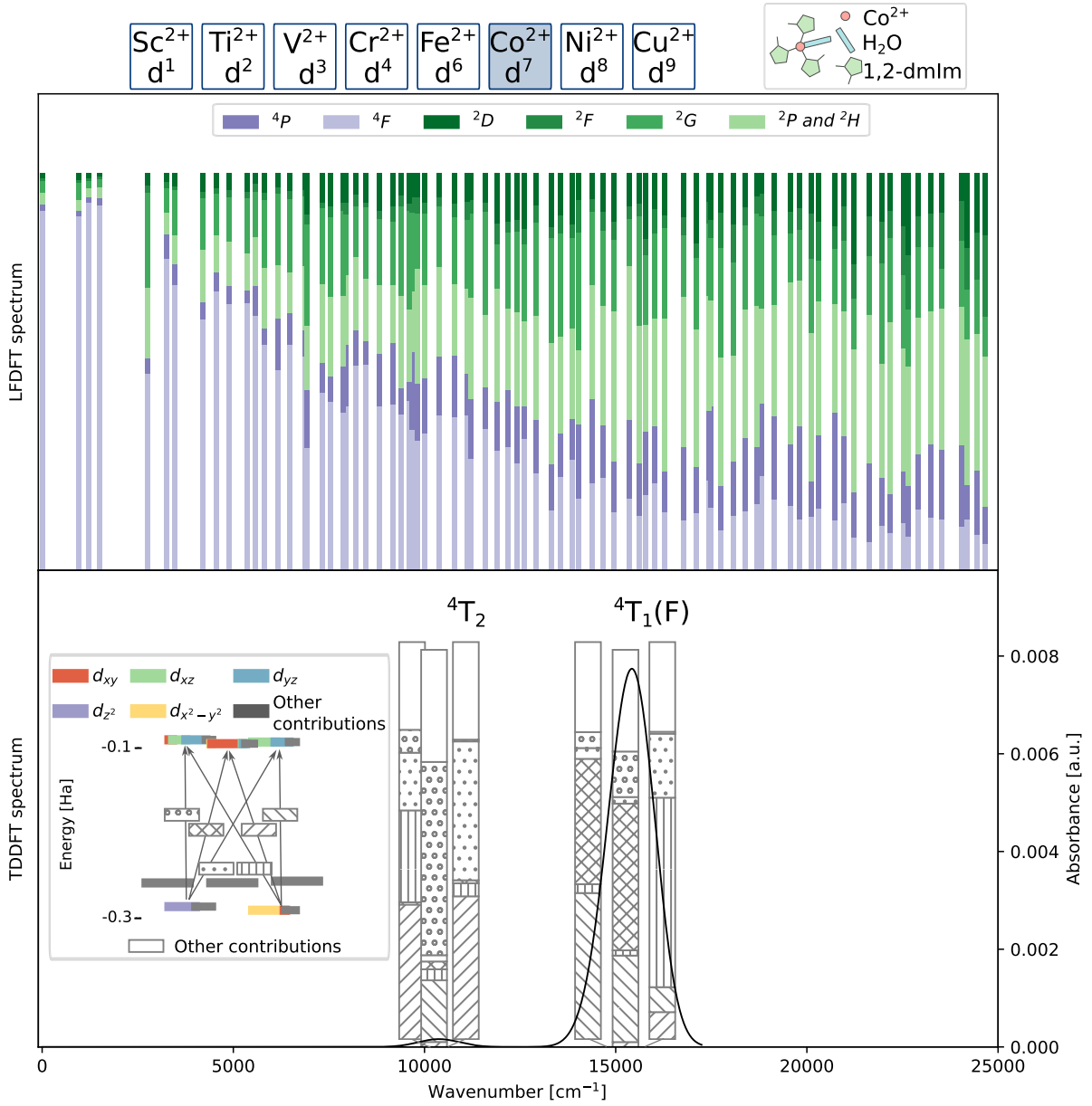

Figure 17. LFDFT (top) and TDDFT (bottom) spectrum of $[Co(1,2\text{-dmIm})_3(OR)]^{2+}$. The vertical bars in the LFDFT spectrum indicate the contribution of each microstate. The degeneracy is not displayed. In the TDDFT spectrum, the vertical bars show the excitations with mainly d−d character, whereby the largest contributions are denoted. The legend for the different hatch types is given in the inset in which the β d-orbital splitting obtained via UDFT is presented. The black curve represents the convoluted absorption spectrum for which the axis is presented on the right.

of determining d−d transitions corresponding with double excitations.

The AILFT(NEVPT2) spectrum of $[Co(1,2\text{-dmIm})_3(H_2O)]^{2+}$ is shown in Figure S29. There are no large differences between this spectrum and the one of $[Co(1,2\text{-dmIm})_4]^{2+}$. As such, we conclude that AILFT(NEVPT2) is more suited to study the tetrahedral complexes with 1,2-dmIm ligands than LFDFT. Nevertheless, the differences observed by Filez between tetrahedral complexes with three and four 1,2-dmIm ligands are not retrieved.

4.2.3. $[Co(OR)_6]^{2+}$. As indicated by yellow in Figure 13, $[Co(OR)_6]^{2+}$ complexes are characterized by their band maximum at 19531 cm^{-1}, corresponding to the $^4T_{1g}(P)$ state. It has a shoulder located at 21277 cm^{-1}, which also corresponds to the $^4T_{1g}(P)$ state. This is in agreement with the results of Banci et al., who found that, in general, $^4T_{1g}(P)$ is situated in between 15500 and 22000 cm^{-1} for octahedral Co^{2+} complexes.[73] Furthermore, she found that $^4T_{2g}$ is situated in the band 6500−10500 cm^{-1}, but as this ES is situated below the experimentally measured range, it is not observed in Figure 13. Finally, octahedral Co^{2+} complexes have a double excited $^4A_{2g}$ state with a lower intensity which is therefore often hidden by $^4T_{1g}(P)$. The $^4A_{2g}$ state is experimentally observed as a small peak around 15400 cm^{-1} in the raw experimental absorption spectrum of Filez et al., presented in Figure S28.

Good agreement is found between the spectrum shown in Figure 13 and experimental data of $[Co(H_2O)_6]^{2+}$ complexes in aqueous solution[9] too. Indeed, in ref 9, the spin-allowed single excitations to $^4T_{2g}$ and $^4T_{1g}(P)$ are situated at 8100 cm^{-1} and at 19400 and 21550 cm^{-1}, respectively and the spin-

https://doi.org/10.1021/acs.inorgchem.3c01355
Inorg. Chem. XXXX, XXX, XXX−XXX

allowed double excitation to $^4A_{2g}$ is located at 16000 cm^{-1}. Finally, the lowest energy doublet state, i.e., ^2E_g, is situated at 11300 cm^{-1}.

We now compare the experimental spectrum shown in Figure 13 to the LFDFT and TDDFT results presented in Figure 12. There is good agreement with the LFDFT spectrum in which $^4T_{2g}$ and $^4T_{1g}(P)$ are situated at 8100−9400 cm^{-1} and 18400−21900 cm^{-1}, respectively. $^4A_{2g}$ is located at 17500 cm^{-1}. It is more difficult to determine the specific excitation energy of ^2E_g as contributions from doublet states are observed at 6600, 8400, and 13600−15700 cm^{-1}. The TDDFT results are also in good agreement: $^4T_{1g}(P)$ is located around 20000 cm^{-1}, whereas there is a slight shift observed for $^4T_{2g}$, which is located at 10000−11300 cm^{-1}.

The AILFT(NEVPT2) spectrum of $[Co(H_2O)_6]^{2+}$ is shown in Figure 18. When comparing with the LFDFT spectrum shown in Figure 12, we note that the spectra are similar, but some differences need to be highlighted. First of all, $^4T_{2g}$ and $^4A_{2g}$ are shifted to smaller energies. Excitation energies of $[Co(H_2O)_6]^{2+}$ determined via the ab initio methods, both CASSCF and NEVPT2, and the LFT models derived from them, AILFT(CASSCF) and AILFT(NEVPT2), are listed in Table S1. The influence of dynamic correlation can be estimated by comparing the CASSCF and NEVPT2 results on the one hand and the AILFT(CASSCF) and AILFT(NEVPT2) results on the other hand. These results reveal that the inclusion of dynamic correlation effects can not be omitted.

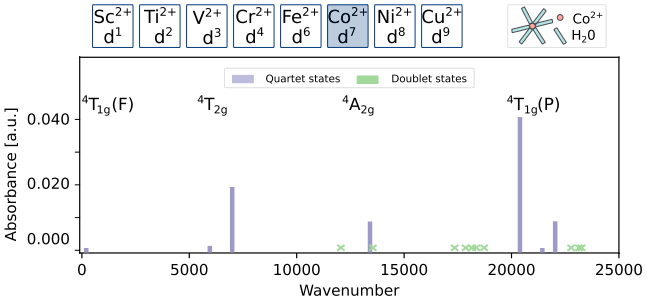

Figure 18. AILFT(NEVPT2) spectrum of $[Co(H_2O)_6]^{2+}$. Quartet states are indicated in purple and their oscillator strength is presented by the height of the bar. The spin-forbidden doublet states are indicated with green crosses and have zero oscillator strength.

4.2.4. Spectroscopic Fingerprint. We are now able to propose a spectroscopic fingerprint to follow the nucleation of Co-ZIF-67. Therefore, we compare the TDDFT spectra, which are shown in Figures 12, 15, and 17 and summarized in Figure 19. Remark that the absorbance is shown on the right axis for $[Co(H_2O)_6]^{2+}$, whereas it is on the left axis for the other complexes. The LFDFT spectra are not considered, as no conclusions can be drawn when the TMC possesses extended ligands. First of all, we note that the oscillator strength of the centrosymmetric octahedral complexes is much smaller than that of tetrahedral TMCs, which accords with experiments. Based on the calculated absorbance shown in Figure 19 and the experimental data shown in Figure 13, the order of magnitude of the ratio of octahedral versus tetrahedral concentrations can be estimated. We found that the tetrahedral complexes that trigger the nucleation process are 10^{-7}−10^{-8} times less present than the octahedral structures. This indicates that there is only a limited number of tetrahedral complexes which trigger the nucleation process. Furthermore, the most intense peak of the octahedral Co^{2+} complexes is situated at larger energies compared to that of the tetrahedral structures, i.e., 20000 versus 15000 cm^{-1}. Generally, these energies are in the correct ranges and strongly align with CFT, in which a smaller Δ is predicted for tetrahedral complexes than for octahedral ones. Besides the main absorption peak, both octahedral and tetrahedral complexes have additional, less intense, ESs around 10000 cm^{-1}. Finally, d−d excitations with very low energies are observed for the octahedral complexes and arise due to the degeneracy of the GS. As the tetrahedral systems have a nondegenerate GS, no d−d excitations are observed in this region. Unfortunately, on the basis of TDDFT

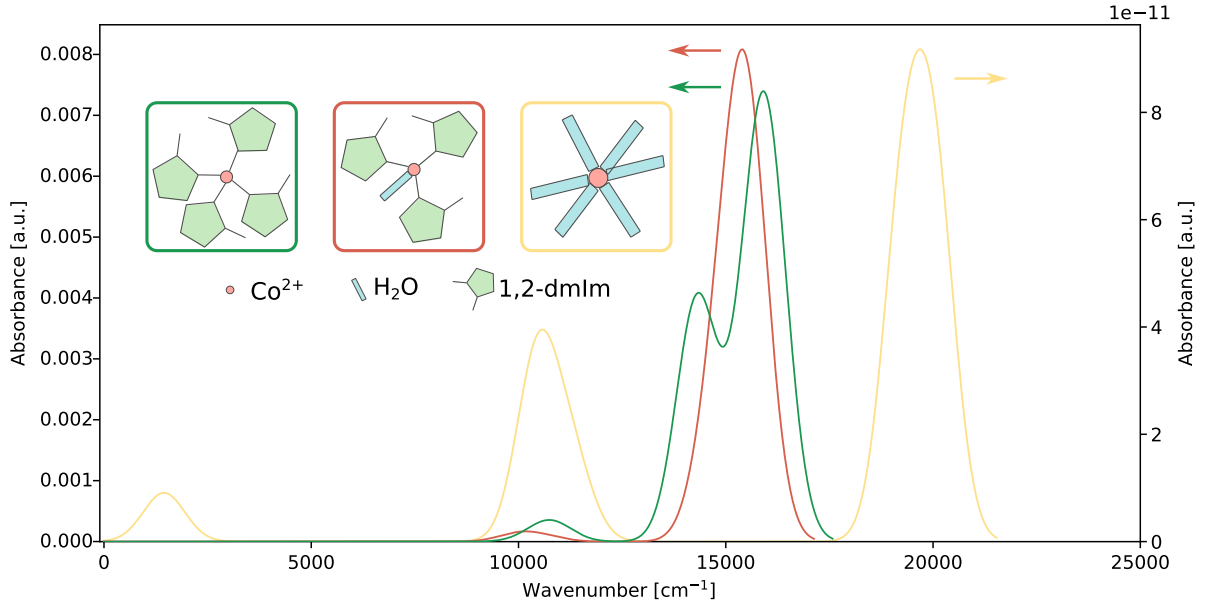

Figure 19. TDDFT spectra of $[Co(H_2O)_6]^{2+}$ (yellow), $[Co(1,2\text{-dmIm})_3(H_2O)]^{2+}$ (red), and $[Co(1,2\text{-dmIm})_4]^{2+}$ (green). The absorbance is on the right for $[Co(H_2O)_6]^{2+}$, whereas it is on the left for $[Co(1,2\text{-dmIm})_3(H_2O)]^{2+}$ and $[Co(1,2\text{-dmIm})_4]^{2+}$.

https://doi.org/10.1021/acs.inorgchem.3c01355
Inorg. Chem. XXXX, XXX, XXX−XXX

calculations, we are not able to calculate the characterizing d−d excitations of $[Co(1,2\text{-dmIm})_3(H_2O)]^{2+}$ and $[Co(2\text{-mIm})_4]^{2+}$ as proposed by Filez et al., as they are double or SF excitations. Therefore, we must emphasize that other techniques are needed which are able to calculate double excitations, in contrast to TDDFT, or which can handle TMCs with extended ligands, as opposed to LFDFT.

5. CONCLUSIONS

In this work, we studied the d−d excitations of Co^{2+} complexes relevant for the nucleation process of Co-ZIF-67 and compared them with experimental spectra in order to investigate how far TDDFT or LFDFT can provide a spectroscopic fingerprint. As it is widely known that the calculation of ESs for TMCs is very challenging, we first focused on octahedral aqua-complexes in order to investigate the challenges encountered when calculating d−d excitations via LFDFT and TDDFT. In the former, one starts from an AOC reference with fractional occupation numbers whereas ESs are calculated from an UDFT GS in the latter. The octahedral aqua-complexes were divided in three categories based on the degeneracy of the GS and the presence of double excitations. The following conclusions have been made. Although the gap between occupied and unoccupied orbitals is overestimated by UDFT compared to AOC, the results of TDDFT and LFDFT are qualitatively in agreement. This even holds for challenging TMCs with a degenerate GS and double excitations. Furthermore, both techniques provide complementary information, double excitations can be studied via LFDFT whereas the oscillator strength can only be retrieved from TDDFT. However, when one wants to make a quantitative comparison, one needs to take in mind that the energies of single ESs interacting with double ESs are overestimated by TDDFT in which double excitations are not included. In addition, the TDDFT spectra of tetrahedral complexes need a significant red-shift to match the LFDFT and experimental results. As we observed that the d−d excitations strongly depend on the chosen functional, the performance of additional functionals could be tested. Finally, care must be taken when TMCs with S_6 symmetry and degenerate GS are studied.

In a second step, we reverted our attention to complexes that are relevant for the nucleation of Co-ZIF-67. These include octahedral Co^{2+} aqua-complexes and tetrahedral Co^{2+} complexes with 2-mIm and aqua ligands. The most prominent difference between the octahedral and tetrahedral Co^{2+} complexes is that the oscillator strengths of the former are much smaller as these systems possess a center of symmetry. A comparison of the ratio of the absorption peaks in experiment and theory allowed us to estimate the ratio of octahedral and tetrahedral complexes. It was found that the tetrahedral structures that trigger the nucleation process are 10^{-7}−10^{-8} times less present than the octahedral complexes. Another way in which the tetrahedral and octahedral TMCs can be distinguished is by the position of the main absorption peak, which is shifted to smaller wavelengths for the former, which is in agreement with CFT. Furthermore, additional ESs are observed at very small energies for the octahedral complex, whereas this is not the case for the tetrahedral structures. Neither TDDFT nor LFDFT was able to differentiate between the $[Co(1,2\text{-dmIm})_4]^{2+}$ and $[Co(1,2\text{-dmIm})_3(H_2O)]^{2+}$ complexes. We found that LFDFT can no longer be used for the tetrahedral complexes containing 2-mIm ligands because the obtained spectra are too spread-out. Therefore, we briefly investigated the performance of AILFT and found, just like for TDDFT, that no large differences are observed between the spectra of $[Co(1,2\text{-dmIm})_4]^{2+}$ and $[Co(1,2\text{-dmIm})_3(H_2O)]^{2+}$. Nevertheless, AILFT is a promising technique to study these complicated systems. As the experimentally proposed fingerprint by Filez et al. is situated in the UV−vis region and contains mainly double and SF excitations, other techniques which are able to include double excitations and can handle TMCs with no symmetry are needed to distinguish between these tetrahedral complexes.

■ ASSOCIATED CONTENT

Supporting Information

The Supporting Information is available free of charge at https://pubs.acs.org/doi/10.1021/acs.inorgchem.3c01355.

Tanabe−Sugano diagrams for octahedral d^2 and d^8 complexes, *d*-orbital splittings obtained with AOC and AILFT, LFDFT, TDDFT, and raw experimental absorption spectra, and geometries of optimized structures (PDF)

■ AUTHOR INFORMATION

Corresponding Author

Veronique Van Speybroeck − *Center for Molecular Modeling (CMM), Ghent University, 9052 Zwijnaarde, Belgium;* orcid.org/0000-0003-2206-178X; Email: Veronique.VanSpeybroeck@UGent.be

Authors

Liesbeth De Bruecker − *Center for Molecular Modeling (CMM), Ghent University, 9052 Zwijnaarde, Belgium;* orcid.org/0000-0001-7844-6932

Matthias Filez − *Conformal Coating of Nanomaterials (CoCooN), Ghent University, 9000 Gent, Belgium;* orcid.org/0000-0002-7810-637X

Complete contact information is available at: https://pubs.acs.org/10.1021/acs.inorgchem.3c01355

Notes

The authors declare no competing financial interest.

■ ACKNOWLEDGMENTS

The authors acknowledge the Research Board of Ghent University (BOF) for funding. The computational resources and services used in this work were provided by VSC (Flemish Supercomputer Center), funded by Ghent University, Fund for Scientific Research Flanders (FWO), and the Flemish Government Department EWI. M.F. acknowledges the FWO for a senior postdoctoral research fellowship (1280621N).

■ REFERENCES

(1) Yao, J.; Wang, H. Zeolitic Imidazolate Framework Composite Membranes and Thin Films: Synthesis and Applications. *Chem. Soc. Rev.* **2014**, *43*, 4470−4493.

(2) Sun, Y.; Rogge, S. M. J.; Lamaire, A.; Vandenbrande, S.; Wieme, J.; Siviour, C. R.; Van Speybroeck, V.; Tan, J.-C. High-Rate Nanofluidic Energy Absorption in Porous Zeolitic Frameworks. *Nat. Mater.* **2021**, *20*, 1015−1023.

(3) Hu, Y.; Kazemian, H.; Rohani, S.; Huang, Y.; Song, Y. In Situ High Pressure Study of ZIF-8 by FTIR Spectroscopy. *Chem. Commun.* **2011**, *47*, 12694−12696.

(4) Filez, M.; Caratelli, C.; Rivera-Torrente, M.; Muniz-Miranda, F.; Hoek, M.; Altelaar, M.; Heck, A. J.R.; Van Speybroeck, V.; Weckhuysen, B. M. Elucidation of the Pre-Nucleation Phase Directing Metal-Organic Framework Formation. *Cell Rep. Phys. Sci.* **2021**, *2*, 100680.
(5) De Bruecker, L.; Van Speybroeck, V. Influence of Number of Ligands and Point Group on the Electronic Structure of $d - d$ Aqua-Complexes. *Inorg. Chem.* **2022**, *61*, 20743.
(6) Neese, F.; Petrenko, T.; Ganyushin, D.; Olbrich, G. Advanced Aspects of Ab Initio Theoretical Optical Spectroscopy of Transition Metal Complexes: Multiplets, Spin- Orbit Coupling and Resonance Raman Intensities. *Coord. Chem. Rev.* **2007**, *251*, 288−327.
(7) Yang, Y.; Ratner, M. A.; Schatz, G. C. Multireference Ab Initio Study of Ligand Field d−d Transitions in Octahedral Transition-Metal Oxide Clusters. *J. Phys. Chem. C* **2014**, *118*, 29196−29208.
(8) Vlahovic, F.; Peric, M.; Gruden-Pavlovic, M.; Zlatar, M. Assessment of TD-DFT and LF-DFT for Study of d−d Transitions in First Row Transition Metal Hexaaqua Complexes. *J. Chem. Phys.* **2015**, *142*, 214111.
(9) Jörgensen, C. K. *Spectroscopy of Transition-Group Complexes in Advances in Chemical Physics*; John Wiley and Sons, Inc., 1963.
(10) Zobel, J. P.; González, L. The Quest to Simulate Excited-State Dynamics of Transition Metal Complexes. *JACS Au* **2021**, *1*, 1116−1140.
(11) Daniel, C.; González, L.; Neese, F. Quantum Theory: The Challenge of Transition Metal Complexes. *Phys. Chem. Chem. Phys.* **2021**, *23*, 2533−2534.
(12) Daniel, C. *Density Functional Theories and Coordination Chemistry*; Elsevier, 2020.
(13) Almeida, N. M. S.; McKinlay, R. G.; Paterson, M. J. Computation of Excited States of Transition Metal Complexes. *Struct. Bonding (Berlin)* **2014**, *167*, 107−138.
(14) Radoń, M.; Drabik, G. Spin States and Other Ligand-Field States of Aqua Complexes Revisited with Multireference ab Initio Calculations Including Solvation Effects. *J. Chem. Theory Comput.* **2018**, *14*, 4010−4027.
(15) Tanabe, Y.; Sugano, S. On the Absorption Spectra of Complex Ions. I. *J. Phys. Soc. Jpn.* **1954**, *9*, 753−766.
(16) Atkins, P.; Overton, T.; Weller, M.; Armstrong, F.; Hagerman, M. *Shriver & Atkins' Inorganic Chemistry*; W. H. Freeman and Company, 2010.
(17) Miessler, G. L.; Fischer, P. J.; Tarr, D. A. *Inorganic Chemistry*; Pearson, 2014.
(18) Griffth, J. S. *The Theory of Transition Metal Ions*; Cambridge University Press, 1961.
(19) Holmes, O. G.; McClure, D. S. Optical Spectra of Hydrated Ions of the Transition Metals. *J. Chem. Phys.* **1957**, *26*, 1686−1694.
(20) Jörgensen, C. K. *Absorption Spectra and Chemical Bonding in Complexes*; Pergamon Press, 1962.
(21) Cullen, J.; Krykunov, M.; Ziegler, T. The Formulation of a Self-Consistent Constricted Variational Density Functional Theory for the Description of Excited States. *Chem. Phys.* **2011**, *391*, 11.
(22) Ziegler, T.; Krykunov, M.; Seidu, I.; Park, Y. C. *Density-Functional Methods for Excited States*; Springer International Publishing, 2016; pp 61−95.
(23) Krykunov, M.; Ziegler, T. Self-Consistent Formulation of Constricted Variational Density Functional Theory with Orbital Relaxation. Implementation and Applications. *J. Chem. Theory Comput.* **2013**, *9*, 2761.
(24) Seidu, I.; Krykunov, M.; Ziegler, T. The Formulation of a Constricted Variational Density Functional Theory for Double Excitations. *Mol. Phys.* **2014**, *112*, 661−668.
(25) Lejaeghere, K.; Bihlmayer, G.; Bjorkman, T.; Blaha, P.; Blugel, S.; Blum, V.; Caliste, D.; Castelli, I. E.; Clark, S. J.; Dal Corso, A.; de Gironcoli, S.; Deutsch, T.; Dewhurst, J. K.; Di Marco, I.; Draxl, C.; Dułak, M.; Eriksson, O.; Flores-Livas, J. A.; Garrity, K. F.; Genovese, L.; Giannozzi, P.; Giantomassi, M.; Goedecker, S.; Gonze, X.; Granas, O.; Gross, E. K. U.; Gulans, A.; Gygi, F.; Hamann, D. R.; Hasnip, P. J.; Holzwarth, N. A. W.; Iusan, D.; Jochym, D. B.; Jollet, F.; Jones, D.; Kresse, G.; Koepernik, K.; Kucukbenli, E.; Kvashnin, Y. O.; Locht, I. L. M.; Lubeck, S.; Marsman, M.; Marzari, N.; Nitzsche, U.; Nordstrom, L.; Ozaki, T.; Paulatto, L.; Pickard, C. J.; Poelmans, W.; Probert, M. I. J.; Refson, K.; Richter, M.; Rignanese, G.-M.; Saha, S.; Scheffler, M.; Schlipf, M.; Schwarz, K.; Sharma, S.; Tavazza, F.; Thunstrom, P.; Tkatchenko, A.; Torrent, M.; Vanderbilt, D.; van Setten, M. J.; Van Speybroeck, V.; Wills, J. M.; Yates, J. R.; Zhang, G.-X.; Cottenier, S. Reproducibility in Density Functional Theory Calculations of Solids. *Science* **2016**, *351*, aad3000.
(26) Mingos, D. M. P.; Day, P.; Dahl, J. P. *Molecular Electronic Structures of Transition Metal Complexes II*; Springer: Berlin, 2012.
(27) Singh, S. K.; Eng, J.; Atanasov, M.; Neese, F. Covalency and Chemical Bonding in Transition Metal Complexes: An Ab Initio Based Ligand Field Perspective. *Coor. Chem. Rev.* **2017**, *344*, 2−25.
(28) Ziegler, T.; Rauk, A.; Baerends, E. J. On the Calculation of Multiplet Energies by the Hartree-Fock-Slater Method. *Theor. Chim. Acta.* **1977**, *43*, 261−271.
(29) Daul, C. Density Functional Theory Applied to the Excited States of Coordination Compounds. *Int. J. Quantum Chem.* **1994**, *52*, 867−877.
(30) Atanasov, M.; Daul, C.; Rauzy, C. New Insights into the Effects of Covalency on the Ligand Field Parameters: a DFT Study. *Chem. Phys. Lett.* **2003**, *367*, 737−746.
(31) Atanasov, M.; Daul, C.; Rauzy, C. A DFT Based Ligand Field Theory. *Struct. Bonding (Berlin)* **2004**, *106*, 97−125.
(32) Atanasov, M.; Daul, C. Modeling Properties of Molecules with Open d-shells Using Density Functional Theory. *C. R. Chim.* **2005**, *8*, 1421−1433.
(33) Atanasov, M.; Comba, P.; Daul, C.; Neese, F. In *Models, Mysteries and Magic of Molecules*; Boeyens, J. C. A., Ogilvie, J. F., Eds.; Springer, 2008; pp 411−445.
(34) Runge, E.; Gross, E. K. U. Density-Functional Theory for Time-Dependent Systems. *Phys. Rev. Lett.* **1984**, *52*, 997−1000.
(35) Casida, M. E.; Jamorski, C.; Casida, K. C.; Salahub, D. R. Molecular Excitation Energies to High-Lying Bound States from Time-Dependent Density-Functional Response Theory: Characterization and Correction of the Time-Dependent Local Density Approximation Ionization Threshold. *J. Chem. Phys.* **1998**, *108*, 4439−4449.
(36) Bauernschmitt, R.; Ahlrichs, R. Treatment of Electronic Excitations Within the Adiabatic Approximation of Time Dependent Density Functional Theory. *Chem. Phys. Lett.* **1996**, *256*, 454−464.
(37) Baer, R. Prevalence of the Adiabatic Exchange-Correlation Potential Approximation in Time-Dependent Density Functional Theory. *J. Mol. Struct. Teochem.* **2009**, *914*, 19−21.
(38) Laurent, A. D.; Jacquemin, D. TD-DFT Benchmarks: A Review. *Int. J. Quantum Chem.* **2013**, *113*, 2019−2039.
(39) Laurent, A. D.; Adamo, C.; Jacquemin, D. Dye Chemistry with Time-Dependent Density Functional Theory. *Phys. Chem. Chem. Phys.* **2014**, *16*, 14334−14356.
(40) González, L.; Escudero, D.; Serrano-Andrés, L. Progress and Challenges in the Calculation of Electronic Excited States. *ChemPhysChem* **2012**, *13*, 28−51.
(41) Cramer, C. J.; Truhlar, D. G. Density Functional Theory for Transition Metals and Transition Metal Chemistry. *Phys. Chem. Chem. Phys.* **2009**, *11*, 10757−10816.
(42) Le Bahers, T.; Bremond, E.; Ciofini, I.; Adamo, C. The Nature of Vertical Excited States of Dyes Containing Metals for DSSC Applications: Insights from TD-DFT and Density Based Indexes. *Phys. Chem. Chem. Phys.* **2014**, *16*, 14435−14444.
(43) Mori, K.; Goumans, T. P. M.; van Lenthe, E.; Wang, F. Predicting Phosphorescent Lifetimes and Zero-Field Splitting of Organometallic Complexes with Time-Dependent Density Functional Theory Including Spin-Orbit Coupling. *Phys. Chem. Chem. Phys.* **2014**, *16*, 14523−14530.
(44) Rosa, A.; Ricciardi, G.; Gritsenko, O.; Baerends, E.. *Principles and Applications of Density Functional Theory in Inorganic Chemistry I*; Springer, 2004; pp 49−116.

https://doi.org/10.1021/acs.inorgchem.3c01355
Inorg. Chem. XXXX, XXX, XXX−XXX

(45) Casida, M. E. In *Recent Advances in Density Functional Methods*; Chong, D. P., Ed.; World Scientific, 1995; p 155.
(46) Bauernschmitt, R.; Ahlrichs, R. Stability Analysis for Solutions of the Closed Shell KohnâĂŞSham Equation. *J. Chem. Phys.* **1996**, *104*, 9047−9052.
(47) Jamorski, C.; Casida, M. E.; Salahub, D. R. Dynamic Polarizabilities and Excitation Spectra from a Molecular Implementation of TimeâĂŘDependent DensityâĂŘ.Functional Response Theory: N_2 as a Case Study. *J. Chem. Phys.* **1996**, *104*, 5134.
(48) van Gisbergen, S. J. A.; Groeneveld, J. A.; Rosa, A.; Snijders, J. G.; Baerends, E. J. Excitation Energies for Transition Metal Compounds from Time-Dependent Density Functional Theory. Applications to MnO_4^-, $Ni(CO)_4$, and $Mn_2(CO)_{10}$. *J. Phys. Chem. A* **1999**, *103*, 6835−6844.
(49) Muniz-Miranda, F.; De Bruecker, L.; De Vos, A.; Vanden Bussche, F.; Stevens, C. V.; Van Der Voort, P.; Lejaeghere, K.; Van Speybroeck, V. Optical Properties of Isolated and Covalent Organic Framework-Embedded Ruthenium Complexes. *J. Phys. Chem. A* **2019**, *123*, 6854.
(50) De Bruecker, L.; Everaert, J.; Van Der Voort, P.; Stevens, C. V.; Waroquier, M.; Van Speybroeck, V. Structural and Photophysical Properties of Various Polypyridyl Ligands: A Combined Experimental and Computational Study. *ChemPhysChem* **2020**, *21*, 2489.
(51) Deeth, R. J. Ligand Field and Density Functional Descriptions of the d-States and Bonding in Transition Metal Complexes. *Faraday Discuss.* **2003**, *124*, 379−391.
(52) Jahn, H. A.; Teller, E. Stability of Polyatomic Molecules in Degenerate Electronic States I. Orbital Degeneracy. *Proc. R. Soc. London A* **1937**, *161*, 220−235.
(53) Shee, J.; Loipersberger, M.; Hait, D.; Lee, J.; Head-Gordon, M. Revealing the Nature of Electron Correlation in Transition Metal Complexes with Symmetry-Breaking and Chemical Intuition. *J. Chem. Phys.* **2021**, *154*, 194109.
(54) Maitra, N. T. Double and Charge-Transfer Excitations in Time-Dependent Density Functional Theory. *Annu. Rev. Phys. Chem.* **2022**, *73*, 117−140.
(55) te Velde, G.; Bickelhaupt, F. M.; Baerends, E. J.; Fonseca Guerra, C.; van Gisbergen, S. J. A.; Snijders, J. G.; Ziegler, T. Chemistry with ADF. *J. Comput. Chem.* **2001**, *22*, 931−967.
(56) Becke, A. D. Density-Functional Thermochemistry. III. The Role of Exact Exchange. *J. Chem. Phys.* **1993**, *98*, 5648.
(57) Lee, C.; Yang, W.; Parr, R. G. Development of the Colle-Salvetti Correlation-Energy Formula into a Functional of the Electron Density. *Phys. Rev. B* **1988**, *37*, 785.
(58) Grimme, S.; Antony, J.; Ehrlich, S.; Krieg, H. A Consistent and Accurate Ab Initio Parametrization of Density Functional Dispersion Correction (DFT-D) for the 94 Elements H-Pu. *J. Chem. Phys.* **2010**, *132*, 154104.
(59) Adamo, C.; Barone, V. Toward Reliable Density Functional Methods Without Adjustable Parameters: The PBE0Model. *J. Chem. Phys.* **1999**, *110*, 6158−6169.
(60) Grimme, S.; Ehrlich, S.; Goerigk, L. Effect of The Damping Function in Dispersion Corrected Density Functional Theory. *J. Comput. Chem.* **2011**, *32*, 1456−1465.
(61) Chan, B.; Gill, P. M. W.; Kimura, M. Assessment of DFT Methods for Transition Metals with the TMC151 Compilation of Data Sets and Comparison with Accuracies for Main-Group Chemistry. *J. Chem. Theory Comput.* **2019**, *15*, 3610−3622.
(62) Weymuth, T.; Couzijn, E. P. A.; Chen, P.; Reiher, M. New Benchmark Set of Transition- Metal Coordination Reactions for the Assessment of Density Functionals. *J. Chem. Theory Comput.* **2014**, *10*, 3092−3103.
(63) Pye, C. C.; Ziegler, T. An Implementation of the Conductor-Like Screening Model of Solvation Within the Amsterdam Density Functional Package. *Theor. Chem. Acc.* **1999**, *101*, 396−408.
(64) van Lenthe, E.; Baerends, E. J.; Snijders, J. G. Relativistic Regular Two-Component Hamiltonians. *J. Chem. Phys.* **1993**, *99*, 4597.
(65) van Lenthe, E.; Baerends, E. J.; Snijders, J. G. Relativistic Total Energy Using Regular Approximations. *J. Chem. Phys.* **1994**, *101*, 9783−9792.
(66) van Lenthe, E.; Ehlers, A.; Baerends, E. J. Geometry Optimization in the Zero Order Regular Approximation for Relativistic Effects. *J. Chem. Phys.* **1999**, *110*, 8943−8953.
(67) Dennington, R.; Keith, T. A.; Millam, J. M. *GaussView*, ver. 5; Semichem, Inc.: Shawnee Mission, KS, 2019.
(68) Shao, Y.; Head-Gordon, M.; Krylov, A. I. The Spin-Flip Approach within Time- Dependent Density Functional Theory: Theory and Applications to Diradicals. *J. Chem. Phys.* **2003**, *118*, 4807.
(69) Rinkevicius, Z.; Vahtras, O.; Agren, H. Spin-Flip Time Dependent Density Functional Theory Applied to Excited States with Single, Double, or Mixed Electron Excitation Character. *J. Chem. Phys.* **2010**, *133*, 114104.
(70) Neese, F. Software Update: The ORCA Program System-Version 5.0. *WIREs Comput. Mol. Sci.* **2022**, *12*, e1606.
(71) Neese, F.; Wennmohs, F.; Becker, U.; Riplinger, C. The ORCA Quantum Chemistry Program Package. *J. Chem. Phys.* **2020**, *152*, 224108.
(72) Barone, V.; Cossi, M. Quantum Calculation of Molecular Energies and Energy Gradients in Solution by a Conductor Solvent Model. *J. Phys. Chem. A* **1998**, *102*, 1995.
(73) Banci, L.; Bencini, A.; Benelli, C.; Gatteschi, D.; Zanchini, C. Spectral-Structural Correlations in High-Spin Cobalt(II) Complexes. *Struct. Bonding (Berlin)* **1982**, *52*, 37−86.
(74) Lever, A. B. P. *Inorganic Electronic Spectroscopy*, 2nd ed.; Elsevier, 1984.

https://doi.org/10.1021/acs.inorgchem.3c01355
Inorg. Chem. XXXX, XXX, XXX−XXX